Open your mind. LUT.
Lappeenranta University of Technology

FACULTY OF TECHNOLOGY
LUT ENERGY
ELECTRICAL ENGINEERING

MASTER'S THESIS

MODELLING OF FAULTS IN LOW-VOLTAGE CABLES

Examiners Prof. Jero Ahola
D.Sc. Antti Pinomaa

Author Victor Otu Hayford

Lappeenranta 2016

Abstract

Lappeenranta University of Technology
LUT School of Energy Systems
Electrical Engineering

Victor Otu Hayford
Modelling of Faults in Low-Voltage Cables
Master's thesis
2016
72 pages, 58 pictures, 9 tables, and 2 appendixes

Supervisors: Professor Jero Ahola,
D.Sc. Antti Pinomaa

Keywords: Underground cable, Cable model, Fault model, Fault characterization, Low voltage.

Power line modelling has become an interesting research area in recent years as a result of advances in the power line distribution network system. Extensive knowledge about the power line cable characteristics can be implemented in a software algorithm in a modern broadband power-line communication modem. In this study, a novel approach for modelling power line cables (AMCMK) based on the broadband impedance spectroscopy (BIS) and transmission line matrix (TLM) techniques is recommended in characterizing a healthy cable and the various faults associated with low-voltage cables for both open and short circuit situation.
Models for different cable conditions are developed and tuned, which include six models for both healthy and faulty cables situations. The models are on the basis of impedance response analysis of the cable. The resulting spectra from the simulations are also cross-correlated to determine the degree of similarities between the healthy cable spectra and their respective faulty spectra.

Acknowledgments

This work was performed under the auspices of the Electrical Engineering Department-Lappeenranta University of Technology within the period of summer 2015 and spring 2016.

I would like to express my deepest gratitude to my supervisor, Professor Jero Ahola, for his guidance and warmly accepting me to work under his supervision.

My sincerest and heartfelt thanks go to my other supervisor D.Sc. Antti Pinomaa for his patience, and constructive criticism that guided me throughout this work. This thesis would not have been possible without his advice and support.

I am immensely grateful to Antti Kosonen (Assoc. Prof.) for his invaluable contribution and intellectual guidance from the beginning to the final moment of this study.

I would like to also thank my special friend Andres Belzunce for his genius advice and always being there when I needed him most.

Finally, my profound gratitude goes to my family for their encouragement, support, and prayers.

Above all, I would like to thank Jehovah God Almighty for the blessings of life, strength, and the wisdom throughout this study.

Table of contents

1 Introduction 1

1.1 Background 1

1.2 Fault in the Low-Voltage Cable and Fault Locating Method 4

1.2.1 Damage Mechanism 4

1.3 State-of-the-Art Analysis for Condition Monitoring and Fault Detection Techniques 9

1.3.1 Mechanical Technique 9

1.3.2 Chemical Technique 10

1.3.3 Electrical Technique 11

1.4 Objectives 16

2 Transmission Line Theory 18

2.1 Transmission Line Circuit Model 18

2.2 Waves on the Transmission Line 19

2.3 Transmission Line Discontinuity 21

2.4 Transmission Chain Parameter Matrix 23

2.5 Determination of Line Parameters by Input Impedance Measurements 26

3 The Low-Voltage Underground Cables 28

3.1 AMCMK LV Power Cable. 28

3.2 AMCMK 3 ½-Core Cable 29

3.3 AMCMK 4 ½ - Core Cable 29

3.4 AXMK Cable 30

4 Input Impedance Measurements 32

4.1 Input Impedance Measurement Setup 32

4.2 Effect of Distributed Parameters on Input Impedance Response 32

4.3 Input-Impedance Analysis 34

5 Modeling of Power Cable - State of the Arts 40

5.1 Top-Down Approach 40

5.2 Bottom-Up Approach 41

5.3 Theory of Broadband Impedance Spectroscopy 41

6 Modeling of AMCMK Power Cable 44

6.1 Model for Healthy Cable 44

6.1 Model for Faulty Cable 49

6.1.1 Model for Phase to Phase Open Circuit Faults 49

6.1.2 Model for Phase to Phase Short Circuit Fault 54

6.1.3 Model for Phase to Ground (L1, PE) Open-Circuit Fault 56

6.1.4 Model for Phase to Ground (L1, PE) Short-Circuit Fault 58

6.2 Analysis of Input Impedance Response Models 60

6.3 Cross Correlation Analysis 63

7 Conclusion 66

References 68

Appendices:

Appendix 1 Algorithm used in modelling the fault

Appendix 2 Figures and Table which were not included in the main text

Symbols

c	distributed capacitance
f	frequency
g	distributed conductance
h	initial coefficient of distributed resistance
i	instantaneous current
k	initial coefficient of distributed conductance
l	distributed inductance
r	distributed resistance
s	standard deviation
u	instantaneous voltage
x	place
$\mathbf{A}$	frequency-dependent coefficient matrix
$\mathbf{B}$	frequency-dependent coefficient matrix
$\mathbf{C}$	frequency dependent coefficient matrix
$\mathbf{D}$	frequency-dependent coefficient matrix
$\mathbf{H}$	transfer function of communication channel
$\mathbf{I}$	current vector
$\mathbf{I}^+$	current propagating to positive direction
$\mathbf{I}^-$	current propagating to negative direction
$\mathbf{I}_{in}$	input current
$\mathbf{I}_{out}$	output current
I_s	source current
L	length of the cable
L_f	fault distance
$\mathbf{T}$	transmission matrix
$\mathbf{U}$	voltage vector
$\mathbf{U}^+$	voltage propagating to positive direction
$\mathbf{U}^-$	voltage propagating to negative direction
$\mathbf{U}_{in}$	input voltage
$\mathbf{U}_{out}$	output voltage
$\mathbf{U}$s	source voltage
$\mathbf{Z}_0$	characteristic impedance
$\mathbf{Z}_{cable,oc}$	input impedance for the cable from the fault location to the cable end
$\mathbf{Z}_{cable,sc}$	input impedance for the cable from the fault location to the cable end
$\mathbf{Z}_f$	fault impedance
$\mathbf{Z}_{in,oc}$	input impedance of cable with other end open circuited
$\mathbf{Z}_{in,sc}$	input impedance of cable with other end short circuited
$\mathbf{Z}_p$	parallel impedance
$\mathbf{Z}_s$	serial impedance, source impedance
$\mathbf{Z}_L$	load impedance

Greek alphabet

α	attenuation coefficient
β	propagation coefficient
$\boldsymbol{\gamma}$	propagation constant
$\varepsilon 0$	permittivity of vacuum

εr	relative permittivity
σ	dielectric conductivity
λ	wavelength
μ0	permeability of vacuum
$\mu_{r,i}$	relative permeability of the insulation material of the transmission
$\epsilon_{r,i}$	relative permittivity of the insulation material of the transmission
ω	angular frequency
$\mathbf{\Gamma}_R$	reflection coefficient

Abbreviations

AC	Alternate current
ACR	Auto-correlation
AMI	Advance metering infrastructure
BIS	Broadband impedance spectroscopy
CCR	Cross-correlation
EAB	Elongation-at-break
EMS	Energy management system
EV	Electric vehicle
CDPV	Contaminants, defects, protrusions, voids
CM	Comprehensive modulus
DV	Distributed generation
DG	Distributed generation
FDR	Frequency-domain reflectometry
FTIR	Fourier transform infrared spectroscopy
IRT	Insulation resistance test
LV	Low voltage
LVDN	Low-voltage distribution network
AMCMK	PVC insulated and sheathed cable with sector shaped, stranded aluminium conductor
OFDM	Orthogonal frequency-division multiplexing
OIT	Oxidation induction time
PD	Partial discharge
PE	Protective earth
PLC	Power line communication

PRBS	Pseudo-random binary sequences
PVC	Polyvinyl chloride
SG	Smart grid
SSTDR	Spread spectrum time domain reflectometry
STDR	Sequence time-domain reflectometry
TDR	Time-domain reflectometry
TEM	Transverse electromagnetic
TLM	Transmission-line matrix
UG	Under ground
VSWR	Voltage standing wave ratio

1 Introduction

Power line (cable) modelling has become an interesting area of research in recent years, especially, in the distribution network sector as it is a way of understanding the complex characteristics of a power line communication channel. An example of power line communication channel characterization can be found in [1] and [2]. Extensive knowledge about the power line characteristics can be implemented in a software algorithm in a modern broadband power-line network for a real-time detection of changes in the power line properties in order to estimate their lifetime for effective maintenance.

This thesis focuses on broadband impedance spectroscopy (BIS) in characterizing an AMCMK low-voltage power cable and it is organized as follows. Chapter 1 introduces the background and the objectives of this thesis. Next, the theory used in this work is presented in Chapter 2. This is followed by a description of AMCMK cable in Chapter 3 with a brief introduction to some other low-voltage underground cables typically used in power distribution grids. In Chapter 4, the effects of the cable distributed parameters on the channel response are analysed. Chapter 5 discusses the state-of-the-art of modelling power cables. Chapter 6 presents the modelling methods for AMCMK cable used in this work. Finally, discussion and a conclusion are presented in Chapter 7.

1.1 Background

Owing to the advances in the reliability of electric power distribution system, the use of underground low-voltage (LV) cabling in the power grid will increase in the future. For instance, in the smart grid (SG) systems, low-voltage distribution networks (LVDN) will require a revamp and the role of its automation will be significant due to advanced metering infrastructure (AMI), small-scale distributed generation (DG) units, charging of electric vehicles (EV), and concept of microgrids (µGs) [3]. Smart grid systems (Figure 1.1) will intelligently integrate the actions of all users, thus, generators, transmitters and consumers' participation in the energy management system (EMS) for efficient delivery of sustainable, economical and secure electricity supply [4].

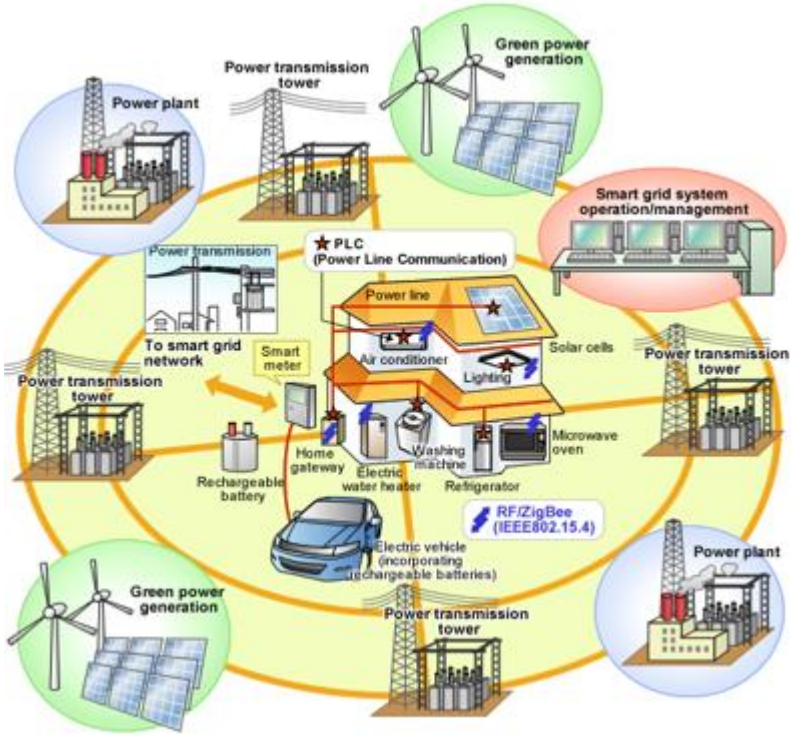

Figure 1.1. Conceptual diagram of a smart grid. [5]

Underground low-voltage cabling is used in some part of a power distribution network system, for example in the utility area since they are hidden from extreme weather conditions and environmental factors such as storms, falling trees etc. to guarantee continuous power supply. As a result of their readily inaccessible nature, an on-line method of monitoring and locating a fault in the underground LV cable has become a necessary and interesting area of study in order to identify faults and also achieve an accurate estimation of their location.

Though underground (UG) cables are buried in the ground, they are not completely immune to adverse weather conditions. They are as well exposed to variant weather conditions which render them susceptible to various faults associated with the electrical power distribution network. For instance, insulation degradation due to the ingress of moisture in the cable insulation material [6] etc.

Detecting faults and maintaining underground LV cables is relatively difficult compered to overhead cables, because of their hidden nature in their installation. Fault locating and condition monitoring in such cables is not a new concept in electrical power distribution system. However, fault and condition monitoring of

such cables can be well evaluated through online measurements. Fortunately, there are several technologies [7] at present that are being implemented in monitoring and locating faults in underground cable networks such as:

- Time-domain reflectometry(TDR)
- Frequency domain reflectometry(FDR)
- Insulation resistance test(IRT)
- Partial discharge (PD)
- Pseudo-random binary sequences(PRBS)
- Spread spectrum time domain reflectometry(SSTDR)
- Sequence time-domain reflectometry(STDR)

Nevertheless, most of the aforementioned techniques are implemented off-line which may only be carried out when there is an actual fault or during scheduled preventive maintenance or condition monitoring program. These off-line techniques over the years especially TDM have proved to be very useful and implemented widely. However, they might not be a good option in the areas where measurements need to be more accurate since their accuracy suffers many drawback for reasons mentioned in Chapter 1.3. For instance, in an SG system where condition monitoring and fault location have to be accurate and also be needed in a real-time situation to avoid a long-time power outage. The use of an on-line method will save time, money and human resource. The on-line method requires algorithms, which scan cables frequently.

Application of a computer-based on-line monitoring system requires an in-depth knowledge about power cable characteristics. According to [8], there are different techniques, which are based on either measurements or theoretical derivations from physical parameters, describe as top-down or empirical models and bottom-up or deterministic models, which can be found in [9].

The work in this thesis focuses on the application of BIS with a transmission line matrices approach in modelling and characterizing an LV cable and some of its associated faults by using information extracted from impedance measurements[10]–[12]. There are several advantages that can be derived from using the BIS method since it is based on broadband impedance response. First, a selection

of the frequency band could be utilised to adjust the range of scanning. Next, faults in the cable and the changes in the insulation materials have much impact on the impedance response. Lastly, it is possible to integrate this method as a software algorithm to modern broadband power-line communication (PLC) modems, which use orthogonal frequency division multiplexing (OFDM), a method where data is encoded on multiple carrier frequencies [12]. It is important noting that, the cable under consideration is an AMCMK low-voltage underground cable and the parameters used in the applied models may have to be tuned for other cable types.

1.2 Fault in the Low-Voltage Cable and Fault Locating Method

Faults in an LV cable can be classified into two main category: open-circuit faults and short-circuit faults. The open-circuit fault occurs mainly due to a break in a conduction path. The second one is the short circuit fault which occurs when there is direct conduction or low resistance between phases and/or the ground [13]. The short-circuit fault can be further divided into symmetrical and unsymmetrical fault. The symmetrical fault occurs when all the phases are short-circuited whereas unsymmetrical means two phases are short-circuited or a situation where the flow of current in the phases are not balanced [14]. These faults are caused by various damage mechanisms. Some of these damage mechanisms are discussed in the next chapter.

1.2.1 *Damage Mechanism*

As indicated earlier, faults in power cables are as a result of various damage mechanisms in which the cables are subjected to within a short (abrupt) and/or long (incipient) period of time. These include aging, mechanical damage, leakage current, treeing, arcing, the presence of voids and impurities in an insulation material. These damage mechanisms act alone or sometimes in the presence of the other. For example, treeing can create low resistance path for leakage current to initiate [6].

Aging

Underground cable usually experiences aging factors, which cause irreversible changes in the property material in an insulation system. This type of aging factors according to [6] are referred to as intrinsic aging. These factors can act alone or with the contribution of the other factors as listed in Table 1.1. For example, damage caused by aging due to environment factor can be found in Figure 1.2.

Another type of aging factor known as extrinsic aging occurs as a result of interaction of the aforementioned aging factors (Table 1.1) with contaminants, defects, protrusions, and voids (CDPV) in the insulation materials. Voids are simply bubbles in the insulation while protrusions are sharp points extending into the insulation. CDPVs may be introduced unintentionally during materials processing, cable manufacturing, transportation, and installation. They can cause a localize change in the uniform material structure. This gradually degrades the insulation, at first, the local area and then to the other parts of the insulation. [6].

Table 1.1. Aging factors in underground cable insulation system [6].

THERMAL	**ELECTRICAL**	**ENVIRONMENTAL**	**MECHANICAL**
Maximum temperature	Voltage (ac, dc, impulse)	Gases (air, oxygen, etc.)	Bending
Low, high ambient temperature	Frequency	Lubricants	Tension
Temperature gradient	Frequency	Water/humidity	Compression
Temperature cycling		Corrosive chemicals	Torsion
		Radiation	Vibration

Figure 1.2. One phase, totally damaged LV underground cable, aluminium oxide broke the sheath [15].

Mechanical Damage

Mechanical damage of power cable are often as a result of incorrect manipulation during the plugging process, excavating, pulling, bending etc. Each of the aforementioned handlings of the power cable can significantly expose the underground cable to a mechanical stress. For example, it is possible to accidentally cause a damage to the cable shield during excavating and ploughing. Excavating can sometimes damage the cable insulation and the conductors. Ploughing can also cause enough damage to the cable shield creating a room for incipient faults as the shield can sustain some degree of cut. Figure 1.3 (a) and (b) shows a totally damage of an LV cable due to incorrect manipulation during the plugging process during installation and a phase damage by multiple screw cut, respectively.

(a) (b)

Figure 1.3. Damaged insulations. (a) Totally damaged insulation material of LV underground cable, caused by incorrect manipulation during the plugging process or installation, (b) insulation material damaged by a screw [15].

Soil Organism

Soil organism such as mole can cause a great deal of damage to underground power cables. This damage mechanism is usually incipient and their late discovery can lead to a more serious one. For instance, exposing the conductors can lead to a short-circuit fault etc. In figure 1.4, when such a damaged cable is exposed to moisture, it renders the cable susceptible to aging through the actions of possible water tree [6].

Figure 1.4. Power cable gnawed by a mole, but still working. Replaced to avoid a future fault. [15]

Voids and impurities in the insulation material

Voids and impurities in the insulation material are the main causes of incipient faults in underground cables [16]. Their existence causes a repeated occurrence of incipient faults, which eventually develop into permanent faults. Voids allow also partial discharge to occur, which deteriorate the insulation of the cable. Partial discharge is usually not expected to occur in LV network, however, the possibility of their presence is never ignored. Deteriorating of the cable insulation can result in a dielectric breakdown and consequently flashover. Figure 1.5 depicts extensive voids in a cable wafer.

Figure 1.5. Cable wafer with extensive voids [17].

Water Treeing

Water trees are known to cause ageing of underground cables. As the name implies, it is a tree-like growth in the insulation material caused by the presence of water or moisture in the cable insulation. They are either initiated at the cables interfaces (vented trees) or grow from the water-filled void or soluble contaminants in the insulation of the cable [6]. In term of aging, water trees that grow from water-filled void do not have significant effect on the breakdown strength of the

cable but at a high temperature, they grow rapidly as a result of moisture diffusion rate. Water trees cause by soluble contaminants according to [6] continue to grow with time but receives little effect from temperature and mechanical stress.

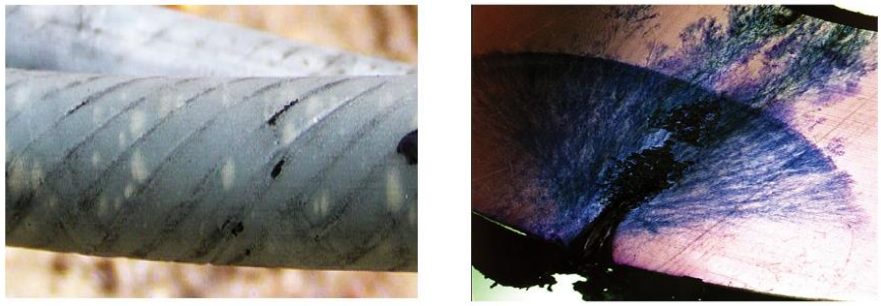

(a) (b)

Figure 1.6. Some evident of water treeing. (a) A cross-linked polyethylene (XLPE) cable with a forest of water trees. (b) A large vented water tree at a fault site. [17]

In Figure 1.6 (b), large vented water tree can be seen growing from the surface of insulation through the insulation layer. Water trees at this state are certain to cause failure. Forest of water trees can also be seen in Figure 1.4 (a), these trees are not cutting through the insulation. It is stated in [17] that water trees need both moisture and the presence of electrical field to grow. Presence of high electrical stress initiates the growth of these trees across the insulation layer to the conductors with time and eventually causes a failure in the cable.

Electrical Treeing

Electrical treeing just like water treeing contributes immensely to the aging and failures in an underground cable. The tree-like channels of this damage mechanism relatively propagate quickly through the insulation causing failure. Electrical treeing is a common fault in a high voltage cable and a source of electrical faults in underground cables. However, it occurs also in low-voltage underground cables. According to [6], an electrical tree can initiate from eroded surfaces in a void, water trees and stress enhancements without voids. The latter has two phases, an initial phase is when applied voltage causes the formation of a void by degrading

the insulation material (Polymer). In the second phase, partial discharge (PD) within the branches causes the voids to extend into a tree-like network channels.

1.3 State-of-the-Art Analysis for Condition Monitoring and Fault Detection Techniques

Review of some condition monitoring and faults detection techniques are highlighted in this section and are categorized into three main sections; mechanical, chemical and electrical. The section is not intended to talk about all condition monitoring techniques but rather to present few which are still current in terms of application.

1.3.1 *Mechanical Technique*

The mechanical technique involves the measurement or monitoring of some physical properties of the cable. This includes visual inspections, elongation-at-break, and compressive modulus measurement [7]. Each of these techniques is discussed below.

Visual Inspection

Visual inspection is an off-line method pertaining to qualitative assessment of the cable in the absence quantitative data. This technique can be used to assess the physical condition of a cable and to also determine if there is the need for extensive testing to effectively characterize its condition. As stated in [7], past studies have confirmed that, in most cases, cables that appear to be in good physical condition through visual inspection show acceptable electrical performance.

The main merit of visual inspection technique is that it is inexpensive to perform and does not require any expensive equipment, only requires human work. To make this kind of technique more effective and consistent, a standardized procedure must be developed and implemented to ensure that all the important cable attributes are inspected. [7]

Elongation-At-Break

According to [7], Elongation-At-Break EAB is defined as a percent increase in elongation at the time of fracture. In this technique, the material resistance to fracture is measured under an applied tensile stress. It is useful in monitoring aging in cable materials due to its sensitivity to microstructural changes in polymers, which occurs as a result of service aging. More details about this technique are presented in [7].

Compressive Modulus

This method is chiefly useful in monitoring the degradation of a cable insulation and jacket materials. Compressive modulus (CM) of a material property is defined as the ratio of compressive stress to compressive strain below the proportional limit [7]. Aging causes insulation and outer jacket material to harden and as a result increases the compressive modulus. Changes in the compressive modulus can be monitored to estimate the rate of degradation of the materials. An instrument for measuring compressive modulus is known as a polymer indenter.

However, to be able to carry out such measurements, the cable need to be accessed just as in the case of the visual inspection. It is most probably not a good method for accessing cable buried underground or laid in a conduit. The only access point, in this case, will be at the terminal but a price has to be paid on the accuracy of the measurements since the terminals might be located at a place with variant ambient conditions.

Application of the polymer indenter in measuring compressive modulus is non-destructive to the normal operation of the power cable as at leaves no physical damage. The whole instrument is computer controlled, however, not all material producing a physical age-induced change in CM can easily be correlated. [7]

1.3.2 *Chemical Technique*

The chemical technique involves the measurement or monitoring of some properties of the cable insulations with regards to changes in their chemistry or molecular

makeup. This includes oxidation induction time (OIT) and Fourier transform infrared spectroscopy (FTIR). OIT technique is explained below and more information about the rest is detailed in [7].

Oxidation Induction Time

Anti-oxidant is one of the constituents of polymeric material used to insulate cable conductor in order to mitigate oxidation that degrades the polymer over time. Unfortunately, anti-oxidant gradually depletes as the cable age due to diffusion and volatilization from the surface. Consequently, continuous depletion of anti-oxidant gradually increases oxidation. By using OIT measurement technique, the time required for a polymer to begin to oxidize is measured under controlled conditions. The measurement value is compared to the value from new cables, this provides an indication of the amount of aging on the cable. However, access to the cable is required to obtain the test specimen. The test must be as well performed in a laboratory setting and the results only provide data on a localized portion of the cable. [7]

1.3.3 *Electrical Technique*

The electrical technique involves the measurement or monitoring of some electrical properties of the cable. This includes spread spectrum time domain reflectometry (SSTDR), sequence time-domain reflectometry (STDR) method, impulse-current method, partial discharge (PD). Each of these techniques is discussed below.

Time-Domain Reflectometry

This technique is used to detect a defect location in a transmission line. According to [18] a known single pulse (a short-time duration pulse) is propagated down a faulty cable under test such that when it reaches the fault termination some of the pulse energy is reflected back to the source (TDR instrument). TDR measures the elapsed time for signal traveling to the end of the cable and the reflections produced by the aforementioned surfaces in the time sequence. This is converted into

distance since the velocity of propagating the pulse is known, approximately between 40%–75 % of the speed of light in a vacuum. The resulting information is displayed as the distance reading. By knowing the cable length, the result can be interpreted as the end of the cable or a fault along the cable.

According to [18], TDR has been in the forefront for cable test measurement. However, it suffers some drawback for fault location estimation. For instance, transmitted pulse progressively broadens and made less sharp due to phase distortion resulting in low resolution of the test outcome. Moreover, the technique is also less susceptible to the link noise interference which can mask out weak distance fault reflection resulting in inaccurate fault location measurement [18]. TDR is, however, a good option for a short distance measurements test and for determining open and short circuit faults and their locations.

Frequency Domain Reflectometry (FDR)

FDR technique is similar to TDR method but quite complex. In FDR, multiple or periodic signals at different frequencies are propagated through the transmission line and the echo channel response is measured in the frequency domain [18], [19]. FDR has a smaller bandwidth compared to TDR. This enhances the quality of the reflected wave by reducing the amount of distortion in it. To show the defect, an impedance spectrum is needed. The impedance spectrum is converted from FDR to TDR using inverse Fourier transform. Incident and reflected wave are then separated with a coupler. The separation can lead to unwanted signal attenuation. This is done over and over again in order to detect the defect. FDR is more effective on dead wire since there will be no noise disturbances in the measuring system. It can achieve a higher signal-to-noise ratio (SNR) by measuring each frequency subsequently. However, it needs a more sophisticated device to perform the measurement in the frequency [19].

Insulation Resistance Test

This is usually performed to determine the conditional level of the cable insulation. Once a voltage is applied from the conductor to the ground, the insulation resistance between the ground and the conductor can be measured. It is inexpensive

and relatively easy to perform. If the insulation resistance decreases in a predictable manner as the insulation ages, trending of this parameter could be useful as a condition monitoring technique for electric cables. [7]

According to [20], for fault-locating techniques on a shielded power cable system, an insulation resistance tester/Ohmmeter may be used to perform insulation resistance test and to locate cable faults. For example, at insulation resistance test voltage level of 500 to 2500 V, with an Ohmmeter test voltage level 1.5 to 9 V, a cable fault can be categorized and the effectiveness of the cable-fault locating technique can be predicted. See appendix 2 (Table 1).

Partial Discharge

This technique is used to determine a defect in an isolation barrier or insulation material. This occurs due to a defect in an insulation material such as voids, cracks or inclusion within a solid dielectric at interfaces within solid or liquid dielectrics, in bubbles within liquid dielectrics or along the boundary between different insulation materials. The defect eventually causes localised ionization when exposed to prolong high voltage. The continuous presence of this ionization deteriorate the insulation material progressively and can lead to an electric breakdown. [21]

Impulse-Current Method

Impulse-current method, unlike TDR, takes advantage of the electrical transient created by a breakdown rather than acoustic transient. This method advantages the use of pulse echo method (TDR) due to its wide range of application, thus, it can be applied to every type of fault. In this method, faults are located by detecting and recording the current signal flowing in the impulse generator circuit using a high-speed digital transient recorder. It falls on the direct reflection of the applied impulse as in the pulse-echo instrument to locate low shunt fault and open circuit series faults. [22]

Sequence Time-Domain Reflectometry Method (STDR)

STDR propagate pseudo-noise (PN) code as a test signal, shown in appendix II Figure 1 (a). This signal is very small and does not interfere with the signal in the

live wire. The nature of the incident signal makes it immune to other noise on the line. The received signal, which is a combination of both reflected and incident signals are correlated with a test copy of PN code [23]. In STDR, the correlation delays, multiply, and sum the signals with the PN code as illustrated in appendix II Figure 1(c). The correlation enables STDR to run better on a live wire compared to some reflectometry method.

The most significant advantage of this system is the ability to run it even on a live wire and also create and store its own dynamic baseline. A baseline interprets when a wire is in good shape and when it is faulty. STDR is capable of analyzing branched network but has the same limitation as in TDR. [23].

Spread Spectrum Time Domain Reflectometry Method

Spread spectrum time-domain reflectometry is an improved version of STDR to measure intermittent fault in a live electrical wires using a digital code. This aid in eliminating any interference during the course of the measurement. SSTDR is a combination of a spread-spectrum technology and time-domain reflectometry technology. This method breaks a single TDR signal into smaller signals (sine wave modulated PN code), each with different frequency, see appendix II Figure 1 (b) [7]. This makes the test signals immune to electrical disturbances and noise. The reflected individual signals are then correlated to produce an accurate result as shown in appendix II Figure1 (d). Beside the immunity to the electrical noise, they are also efficient and exhibit low power which guarantees safety for the measurements equipment.

Correlation Pulse Echo Techniques: Pseudo-Random Binary Sequences (PRBS)

PRBS has been developed as an alternative to TDR technique. This is meant to clearly identify the nature of the fault and its actual location. In this technique, the PRBS test perturbation is cross-correlated (CCR) with the fault echo response in order to identify the fault and its distance along the line if there is any otherwise the load impedance. In TDR, the measurement technique relies on a single pulse signal which is propagated down a cable as explained earlier on, this technique is not perfect for locating fault because it suffers from attenuation. However by using

wide pulses TDR becomes useful for long distance measurements due to a low rate of signal attenuation. This also suffers from inaccurate long distance resolution. PRBS, on the other hand, utilizes a random code of bipolar pulses that are reflected due to impedance mismatch as a CCR response. The technique compares CCR evaluation of the fault response with injected PRBS and compares the phase shift peak with the auto-correlated peak (ACR-incident sequence signal) to estimate the fault location. A typical example is presented in [18].

Table 1.2. Summary of the various measuring and monitoring techniques by their advantages and disadvantages.

TECHNIQUES	**ADVANATGE**	**DISADVANTAGE**
Visual Inspection	Inexpensive to perform. Use to assess the physical condition of a cable.	Technique needs a standardized procedure for effective and consistent measurement
Elongation-At-Break	A widely accepted measure of polymer aging due to its sensitivity to microstructural changes. Used as a reference in evaluating other techniques	It is a destructive test, and relatively large amounts of a cable is required as cable need to be removed from service, or if there are available sacrificial cable samples for periodic evaluation.
Compressive Modulus	Good for monitoring cable insulation and outer jacket. Non-destructive to the normal operation of the power cable.	Needs cable access making it unsuitable for underground cable.
Oxidation Induction Time	ability to determine cable condition	Cable access is required. Test need a laboratory setting. Results only provide data on a localized portion of the cable
Time-Domain Reflectometry	Uses narrow/wide pulses. Simple, easy to use, widely used. Good option for a short distance measurement test. Good for estimating open and short circuit faults and their locations	Uses narrow pulses which suffers from attenuation over distance. Also wide pulses but suffers from resolution and accuracy. Less susceptible to the link noise interference

Frequency Domain Reflectometry	Smaller bandwidth which enhances the result. Can achieve higher signal-to-noise ratio. Effective on a dead wire.	Procedure complex and can lead to signal attenuation and needs more sophisticated device to perform experiment
Insulation Resistance Test	Ability to determine insulation condition and cable fault in some cases	wide range of application, thus, it can be applied to every type of fault
Partial Discharge	Good for determining defect in an isolation barrier or insulation material	Requires the measurement of small current pulses (<5 pC) while applying a relatively high test voltage
Impulse-Current Method	Wide range of application	
Sequence Time-Domain Reflectometry Method	Small signal which does not interfere with a signal on life wire. It immune to other noise on the line. Runs better on a live wire.	Suffers from attenuation
Spread Spectrum Time Domain Reflectometry Method	Test signal is immune to electrical interfering. Efficient and produces an accurate result. Exhibit low power that guarantees safety. Effective in locating defect on a live wire	Inaccurate long distance resolution.
Correlation Pulse Echo Techniques: Pseudo-Random Binary Sequences	Uses digital code that helps to eliminate any interfering during measurement.	unlikely to accurately reflect any steady state due to a persistent excitation

1.4 Objectives

The main objective of this thesis is to develop a cable and fault models with an algorithm based on the impedance measurements data. These models can be used as an integral part of a software algorithm in a modern broadband power line communication modems, which utilises orthogonal frequency-division multiplexing (OFDM) as a channel access method. To achieve this, a study of novel candidate for cable diagnosis, estimation of fault location and characterization refer to as a

broadband impedance spectroscopy (BIS) is applied. This method is based on broadband impedance response of a power line. A study on the impedance responses analysis of both healthy and faulty AMCMK low-voltage underground cable are implemented in developing the healthy and faulty cable models.

2 Transmission Line Theory

A transmission line (TL) provides a path for propagation of an electromagnetic wave. In transmission line theory, a signal injected into the line propagate as a transverse electromagnetic wave (TEM) [10]. The line is also considered uniform and depending on the wavelength of the transmission line, the geometry of transmission lines can differ from one application to the other as can be seen in Figure 2.1. For instance, applications that require few centimeter of the transmission line as in an electronic circuit such as PC boards, micro-strips (d) and strip-lines (e) are used. On the other hand, applications such as industrial and house wiring as well as intercontinental communications that require long distance communication use coaxial cable (a), two-wire line (b) and fiber optic (c). Waveguide are used mainly to transmit a large amount of microwave over a short or moderate distance [24].

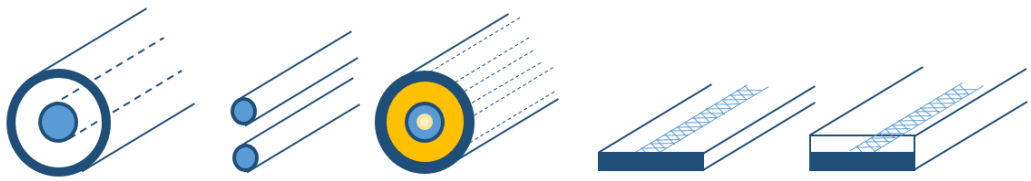

(a) (b) (c) (d) (e)

Figure 2.1. Examples of transmission lines: (a) Coaxial cable, (b) Two-wire line, (c) Optical fiber, (d) Microstrip, (e) Stripline

2.1 Transmission Line Circuit Model

According to [10], in order to solve voltage and current equations in each point of the transmission line, information about the terminal conditions have to be known. Since the low voltage power cable and for that matter the AMCMK cable is a multi-conductor cable, in an industrial environment, for example, all load impedances and their sources need to be modelled with all the phases and the protective earth. This will be difficult to achieve since the phases of the cable cannot be generally considered independent of each other.

Due to the applied signal coupling in this study, where the coupling is between phase one (L1) and phase two (L2) or phase one (L1) and the ground (protective earth-PE), the simplified two-port model has been selected and this neglects the effect of the other conductors not used in the impedance measurements. This is discussed later in Chapter 4.1. Thus, the circuit model (Figure 2.2) and transmission line equations are based on the two-conductor transmission line. As it can be seen in Figure 2.2, the transmission line is assumed to be two-conductor with continuously distributed parameters. The transmission line is considered short when the electrical length is less than one-sixteenth or one-eighth of the wavelength ($l<\lambda/16$ or $l<\lambda/8$) [10], where λ is the wavelength and l the electrical length of the line.

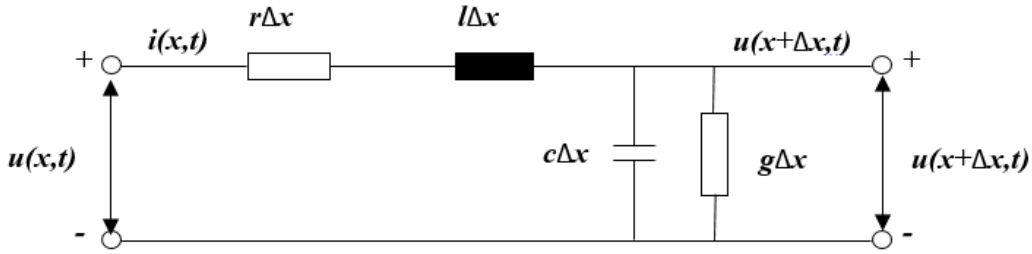

Figure 2.2. Equivalent circuit of differential length Δx of a two-conductor transmission line model with instantaneous signals $u(x,t)$, $u(x+\Delta x,t)$, $i(x,t)$ and $i(x+\Delta x)$ at location x and $x+\Delta x$ in time t [10].

2.2 Waves on the Transmission Line

The waves of the energy being transmitted from the transmitting end to the receiving end of the transmission line according to the circuit model (Figure 2.2) are represented by the following two partial differential equations [1].

$$\frac{du(x,t)}{dt} = -ri(x,t) - l\frac{di(x,t)}{dt} \tag{2.1}$$

$$\frac{di(x,t)}{dt} = -gu(x,t) - c\frac{du(x,t)}{dt} \tag{2.2}$$

where u and i denote instantaneous voltage and current at location x and $x+\Delta x$. Both (2.1) and (2.2) are a function of the position (x) and time (t) which primarily

depends on the distributed parameters *r*, *l*, *g*, and *c* presented, denoting the resistance, inductance, conductance, and capacitance respectively. Due to their infinitesimal nature, they are expressed as a unit per meter. Expressing the above equations in general solution of ordinary differential equation yields:

$$\mathbf{U}(\mathrm{x}) = \mathbf{U}^{+}\mathrm{e}^{-\boldsymbol{\gamma}x} + \mathbf{U}^{-}\mathrm{e}^{\boldsymbol{\gamma}x} \tag{2.3}$$

$$\mathbf{I}(\mathrm{x}) = \frac{1}{\mathbf{Z_0}}(\mathbf{U}^{+}\mathrm{e}^{-\boldsymbol{\gamma}\mathrm{x}} - \mathbf{U}^{-}\mathrm{e}^{\boldsymbol{\gamma}\mathrm{x}}) \tag{2.4}$$

where **U** is the voltage vector establish between the two wires and **I** is the current flowing through them. $\mathbf{Z_0}$ represents the characteristics impedance of the cable and $\boldsymbol{\gamma}$ represents the propagation constant. These two elements of the transmission line define the characteristics of the transverse electromagnetic wave travelling on the transmission line.

The characteristics impedance of the transmission line is given by:

$$\mathbf{Z}_0 = \sqrt{\frac{r+j\omega l}{g+j\omega c}} \tag{2.5}$$

The propagation constant ($\boldsymbol{\gamma}$), which on the other hand defines the attenuation coefficient (α) and the propagation coefficient (β) is given by:

$$\boldsymbol{\gamma} = \sqrt{(r+j\omega l)(g+j\omega c)} = \alpha + j\beta \tag{2.6}$$

When a transmission line is lossless, it means that both distributed resistance *r* and conductance *g* are zero (*r*=*g*=0). Thus, the characteristics impedance only depends on the inductance and the capacitance of the transmission line. $\boldsymbol{Z}_0$ in (2.5) now becomes,

$$\boldsymbol{Z}_0 = \sqrt{\frac{l}{c}} \tag{2.7}$$

while the propagation ($\boldsymbol{\gamma}$) becomes,

$$\boldsymbol{\gamma} = \omega\sqrt{lc} = j\beta \qquad (\alpha = 0) \tag{2.8}$$

The velocity of propagation (v_p) is given by

$$\boldsymbol{v}_p = \frac{1}{\sqrt{lc}} = \frac{1}{\sqrt{\mu_0\mu_{r,i}\epsilon_0\epsilon_{r,i}}} = \frac{\omega}{\beta} \tag{2.9}$$

where μ_0 and ϵ_0 are the relative permeability and permittivity of a free space respectively. Where $\mu_{r,i}$ and $\epsilon_{r,i}$ are relative permeability and permittivity of the insulation material of the transmission

2.3 Transmission Line Discontinuity

The phenomena of a transmission line discontinuity occur when there is an impedance mismatch in the transmission line medium. The mismatch is caused by different impedance termination of the transmission line, for example, different load impedance at the end of the transmission line [10], change in the transmission medium (cable), damage to the cable physical structure, joint etc. [15]. At the point of discontinuity, part of the power delivered by the travelling wave is reflected back to the source while the rest passes through as shown in Figure 2.3.

According to [10], this reflection decreases the performance of the signal for data communication application. It produces standing current and voltage waves ((2.2) and (2.3)) due to the interactions between the sending waves and the reflected waves. The standing waves increase power losses while causing variation in the frequency of the input impedance of the cable terminated by the load impedance. Equation (2.10) shows the complex reflection coefficient $\boldsymbol{\Gamma}_{\mathrm{R}}$ for a transmission line. The reflection coefficient determines the degree of reflection [25] and is expressed by using the complex load impedance $\mathbf{Z}_{\mathrm{L}}$ and the characteristic impedance $\mathbf{Z}_0$.

$$\mathbf{\Gamma}_R = \frac{(\mathbf{Z}_L - \mathbf{Z}_0)}{\mathrm{Z}_L + \mathrm{Z}_0} = |\mathbf{\Gamma}_R| e^{j\theta} \tag{2.10}$$

When $\mathbf{Z}_L = \mathbf{Z}_0$, the reflection coefficient $\mathbf{\Gamma}_R = 0$, thus, in a perfectly matched situation and when the length of the transmission line is infinite [11]. Any other case will cause a reflection due to impedance mismatch.

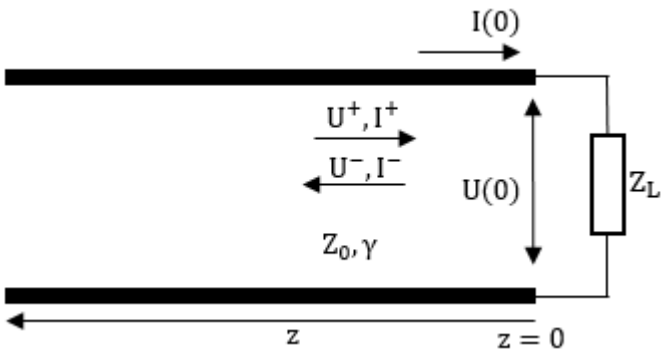

Figure 2.3. Reflection of power at complex load impedance due to impedance mismatch at the load and the cable interface, where $\mathbf{U}^+, \mathbf{I}^+, \mathbf{U}^-, \mathbf{I}^-$ denote voltage and current travelling waves in both positive and negative directions, respectively.

The sinusoidal voltage and current along the length *z* in Figure 2.3 is expressed as

$$\mathbf{U}(z) = \mathbf{U}^+ e^{j\gamma z}(1 + \mathbf{\Gamma}_R e^{-j2\gamma z}) \tag{2.11}$$

$$\mathbf{I}(z) = \frac{\mathbf{U}^+}{\mathbf{Z_0}} e^{j\gamma z}\left(1 - \mathbf{\Gamma}_R e^{-j2\gamma z}\right) \tag{2.12}$$

The amount of impedance mismatch at the load and the line impedance interface can be express by the voltage standing wave ratio (VSWR)

$$\mathrm{VSWR} = \frac{1 + |\mathbf{\Gamma}_R|}{1 - |\mathbf{\Gamma}_R|}. \tag{2.13}$$

where VSWR and $\mathbf{\Gamma}_R$ represent the voltage standing wave ratio and the reflection coefficient respectively.

VSWR and $\mathbf{\Gamma}_R$ are very useful in providing information about the type of line fault present. According to [25], there are four general cases of the line termination that

can occur to influence VSWR and $\boldsymbol{\Gamma}_R$ values. For a matched load condition where the load impedance $\mathbf{Z}_\mathrm{L} = \mathbf{Z}_0, \boldsymbol{\Gamma}_\mathrm{R} = 0$ indicating no reflection with VSWR =1. When there is open-circuit in the line implies $\mathbf{Z}_\mathrm{L} = \infty, \boldsymbol{\Gamma}_\mathrm{R} = -1$. This results in complete incident wave reflection without reversal of the phase. In the case of short-circuit $\mathbf{Z}_\mathrm{L} = 0$ and this results in complete incident wave reflection with the phase reversal. Finally, for a mismatch situation where $\mathbf{Z_L} \neq 0$ complete incident wave will occur with or without phase reversal depending on the relative sizes of the characteristics impedance and the terminated load impedance. Thus, when $\mathbf{Z_L} < \mathbf{Z}_0$ implies $\boldsymbol{\Gamma}_\mathrm{R} < 0$ and **VSWR**= $\mathbf{Z}_0/\mathbf{Z}_\mathrm{L}$. On the other hand, when $\mathbf{Z}_\mathrm{L} > \mathbf{Z}_0$ implies $\boldsymbol{\Gamma}_\mathrm{R} > 0$ and VSWR= $\mathbf{Z}_\mathrm{L}/\mathbf{Z_0}$.

2.4 Transmission Chain Parameter Matrix

The transmission chain parameter matrices are commonly used to model transfer function of a communication channel [10] [12]. However, its application can be utilized to analyze transverse electromagnetic waves as well. TEM waves have transversal electrical and magnetic field only with no longitudinal field [12]. For a two-port network, the relationship between input current $\mathbf{I}_\mathrm{in}$ and voltage $\mathbf{U}_\mathrm{in}$ and output $\mathbf{I}_\mathrm{out}$ current and voltage $\mathbf{U}_\mathrm{out}$ is illustrated in Figure 2.4 and in (2.14).

$$\begin{bmatrix} \mathbf{U}_\mathrm{in} \\ \mathbf{I}_\mathrm{in} \end{bmatrix} = \begin{bmatrix} \mathbf{A} & \mathbf{B} \\ \mathbf{C} & \mathbf{D} \end{bmatrix} \begin{bmatrix} \mathbf{U}_\mathrm{out} \\ \mathbf{I}_\mathrm{out} \end{bmatrix} \tag{2.14}$$

where **A, B, C** and **D** are frequency dependent coefficients.

The frequency dependent input impedance $\mathbf{Z_{in}}$ of the two-port network (Figure 2.4) is given by

$$\mathbf{Z_{in}} = \frac{\mathbf{AZ_L+B}}{\mathbf{CZ_L+D}} \tag{2.15}$$

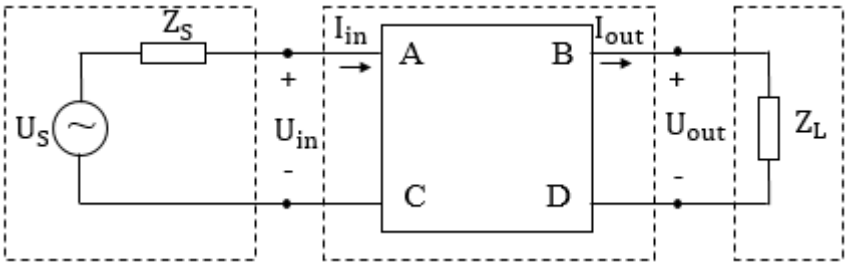

Figure 2.4. Two-port network connected signal source and the load impedance. The signal source comprises voltage source and serially connected internal impedance.

The transfer function of the channel can now be written as

$$\mathrm{H} = \frac{\boldsymbol{U}_{\mathrm{out}}}{\boldsymbol{U}_{\mathrm{S}}} = \frac{\mathbf{Z}_{\mathrm{L}}}{\mathbf{A}\mathbf{Z}_{\mathrm{L}}+\mathbf{B}+\mathbf{C}\mathbf{Z}_{\mathrm{L}}\mathbf{Z}_{\mathrm{S}}+\mathbf{D}\mathbf{Z}_{\mathrm{S}}} \tag{2.16}$$

Coefficients of the transmission matrix depend on the type of the load. The transmission matrix of a transmission line can be illustrated as

$$\begin{bmatrix} \mathbf{A} & \mathbf{B} \\ \mathbf{C} & \mathbf{D} \end{bmatrix} = \begin{bmatrix} \cosh(\boldsymbol{\gamma} L) & \mathbf{Z}_0 \sinh(\boldsymbol{\gamma} L) \\ \frac{1}{\mathbf{Z}_0}\sinh(\boldsymbol{\gamma} L) & \cosh(\boldsymbol{\gamma} L) \end{bmatrix} \tag{2.17}$$

Figure 2.5 (a) and (b) illustrate two-port impedance models for serially connected impedance and parallel connected impedances, respectively. Their respective transmission matrix can be seen in (2.18) and (2.19).

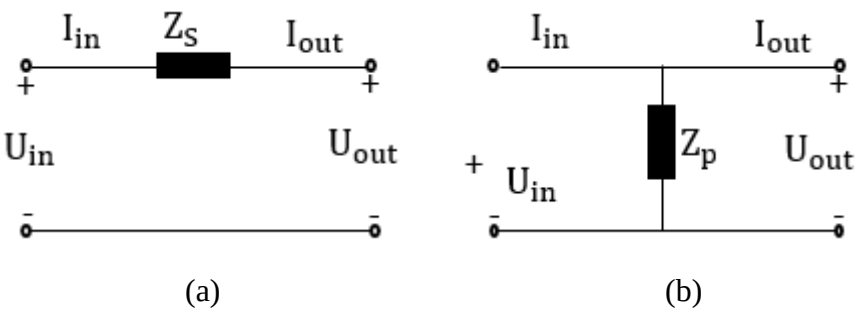

Figure 2.5. Two port impedance model for serial (a) and parallel (b) impedance

Transmission matrix for serially connected impedance $\mathbf{Z}_{\mathrm{S}}$

$$\begin{bmatrix} \mathbf{A} & \mathbf{B} \\ \mathbf{C} & \mathbf{D} \end{bmatrix} = \begin{bmatrix} 1 & \mathbf{Z}_S \\ 0 & 1 \end{bmatrix} \tag{2.18}$$

Transmission matrix for parallel-connected impedance $\mathbf{Z}_P$

$$\begin{bmatrix} \mathbf{A} & \mathbf{B} \\ \mathbf{C} & \mathbf{D} \end{bmatrix} = \begin{bmatrix} 1 & 0 \\ 1/\mathbf{Z}_P & 1 \end{bmatrix} \tag{2.19}$$

The transmission channel from the source to the load may consist of several network sections. Each section need to be represented by its own transmission matrix. Generally, these sections are connected to each other serially as shown in Figure 2.6. The transmission matrix **T** from the source to the load can be simply described by a chain rule

$$\mathbf{T} = \prod_{i=1}^{n} \mathbf{T}_i \tag{2.20}$$

The total transmission matrix for the transmission line from the source to the load (Figure 2.6) can be written in a cascade form as

$$\mathbf{T} = \mathbf{T_1} * \mathbf{T_2} * \mathbf{T_3} * \mathbf{T_4} \tag{2.21}$$

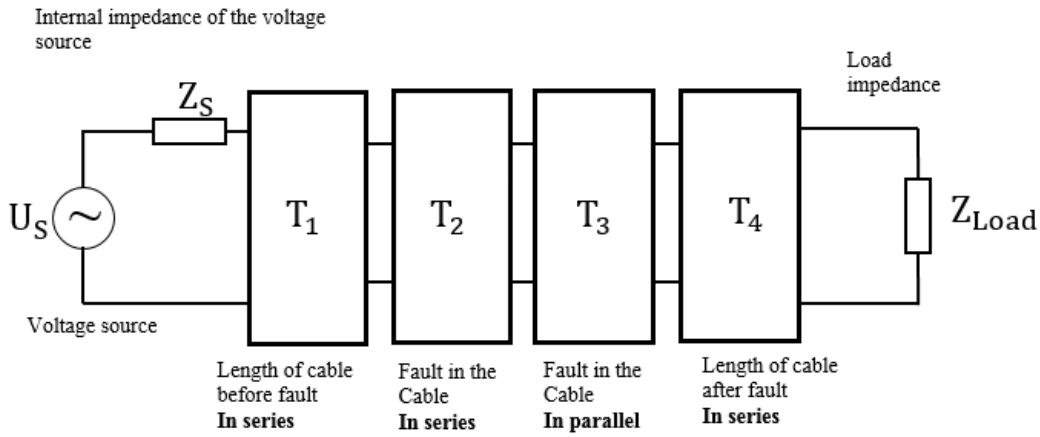

Figure 2.6. Transmission-matrix-base channel model for cable with serial and parallel fault.

2.5 Determination of Line Parameters by Input Impedance Measurements

The characteristics impedance, the propagation constant, and the cable parameters can be determined by performing input impedance measurements for the cable when the ends are open and short-circuited. When the cable ends are left open, the current at the cable end is zero and when is it short-circuit the voltage at the end is zero. The complex input impedance for the open circuit $\mathbf{Z}_{\mathrm{in,oc}}$ and short-circuit $\mathbf{Z}_{\mathrm{in,sc}}$ with the cable length L is given by (2.22) and (2.23) respectively.

$$\mathrm{Z}_{\mathrm{in,oc}} = \mathbf{Z}_0 \mathrm{cotanh}(\boldsymbol{\gamma} L), \tag{2.22}$$

$$\mathrm{Z}_{\mathrm{in,sc}} = \mathbf{Z}_0 \tanh(\boldsymbol{\gamma} L). \tag{2.23}$$

The characteristics impedance $\mathbf{Z}_0$ of the line can be derived from (2.22) and (2.23)

$$\mathbf{Z}_0 = \sqrt{\mathbf{Z}_{\mathrm{in,oc}}\, \mathbf{Z}_{\mathrm{in,sc}}}\,. \tag{2.24}$$

The propagation constant $\boldsymbol{\gamma}$ can now be written as

$$\boldsymbol{\gamma} = \frac{1}{\mathbf{L}} \arctan \sqrt{\frac{\mathbf{Z}_{\mathrm{in,sc}}}{\mathbf{Z}_{\mathrm{in,oc}}}} \tag{2.25}$$

The real part of the propagation constant represents the attenuation coefficient α and the imaginary part represents the propagation coefficient β as shown in (2.6). The distributed inductance l and the capacitance c of the cable can be derived from the characteristic impedance $\mathbf{Z_0}$ and the propagation constant $\boldsymbol{\gamma}$ from (2.24) and (2.25), respectively, by

$$l = \frac{\mathrm{Im}[\mathbf{Z_0}\boldsymbol{\gamma}]}{\omega} \tag{2.26}$$

$$c = \frac{\mathrm{Im}\left[\frac{\boldsymbol{\gamma}}{\mathbf{Z_0}}\right]}{\omega} \tag{2.27}$$

The attenuation coefficient α which determines the losses of the cable, consists of distributed resistance r and the conductance g and is defined by [12]

$$\alpha = \mathrm{Re}[\boldsymbol{\gamma}] \tag{2.28}$$

3 The Low-Voltage Underground Cables

In a typical electricity distribution system network, there are many options with regards to cable selection and the method at which they are deployed [15]. One such method is the underground LV cabling. The underground LV cable is available in a broad variety ranging from three phase to single phase with either carrying or non-carrying concentric neutral and variant protective sheathes or insulation materials. The material for the conductors are also diversified; for example, copper aluminium or alloys [26]. Three-phase underground low-voltage power cable is a multi-conductor cable with three or more core conductors. The underground LV cables carry many advantages, for example, low maintenance costs and less exposure to hash weather condition. However, finding faults occurring in such cables are quite complicated and challenging. This thesis work focuses on underground LV AMCMK power cable. Examples of low-voltage underground cable typically found in the market are Draka AMCMK 4-core [27], Draka AMCMK 3 ½-core, AMCMK 4 ½-core Draka [28] and Nexan AXMK 1 kV [29].

3.1 AMCMK LV Power Cable.

The AMCMK low voltage cable is composed of PVC outer jacket-1 and a concentric layer of copper wire (screens), which act as both protective earth (PE) and the neutral-2. It has plastic filling-3 and PVC insulation-4 around each phase conductor-5 as shown in Figure 3.1. The conductors are up annealed copper.The cross-sectional area of the phase conductor is between 2.5–16 mm^2 [10]. AMCMK cable is rated for a nominal voltage of 1kV. The colours of the conductors' insulation are black, brown and grey in accordance with the HD 308 S2: 2002. In Table 3.1, some physical and electrical characteristics of AMCMK LV power cables are presented with other underground LV cables in the market.

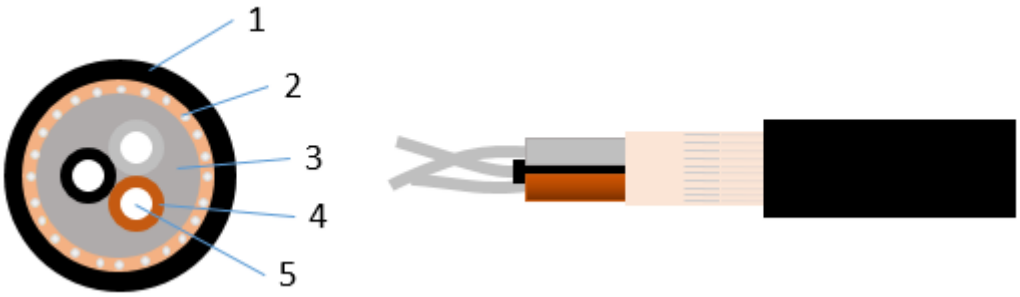

Figure 3.1. Structure of AMCMK low voltage power cable [28].

3.2 AMCMK 3 ½-Core Cable

Like AMCMK (Figure 3.2), the AMCMK 3 ½-Core cable consists of PVC outer jacket-4, a concentric layer of copper wire (screens) which act as both protective earth (PE) and the neutral-2. The core comprises a compacted and annealed sector shaped insulated (PVC) stranded aluminum phase conductors-1. Covering them is concentric copper wire layer-2 which serves as a protective earth (PE). Between the conductor's insulation (PVC) and the concentric copper layer (PE), there is a thin plastic film-3 for protecting cables from moisture and other external substances [17]. The colours of the conductors follow the HD 308 2002 colour S2: standard. This is shown in Figure 3.2.

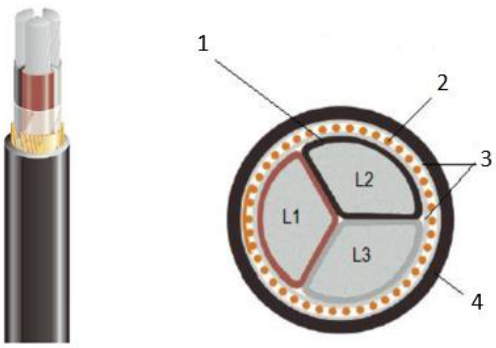

Figure 3.2. Structure of AMCMK 3 ½-Core low voltage power cable.

3.3 AMCMK 4 ½ - Core Cable

Figure 3.3 shows an AMCMK 4 ½-core cable. It is made up compacted and annealed sector-shaped insulated (PVC) aluminum phase conductors and a neutral

conductor stranded together-1. Around the conductors is a concentric copper wire layer and copper tape binding-4 which serve as a protective earth (PE). The cable is enveloped with a black PVC compound shield-5 with outer protective cover. Between the conductors' insulation (PVC) and the concentric copper layer (PE), there is a thin plastic film-3 for protecting cables from moisture and other external substances.

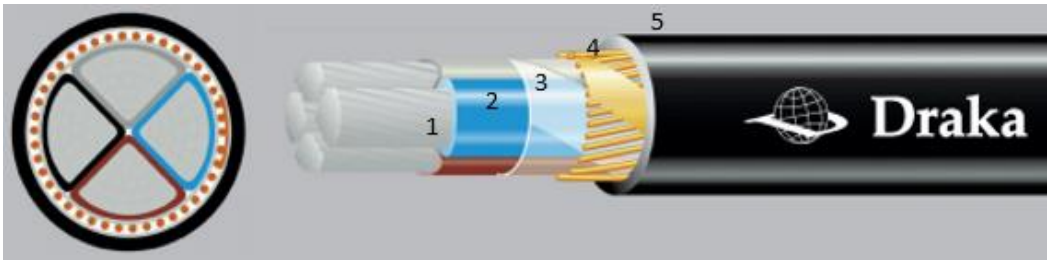

Figure 3.3. Structure of AMCMK 4 ½-Core low voltage power cable [28].

3.4 AXMK Cable

The AXMK cable comprises PVC-sheathed (PEX isolated) outer jacket and most often a concentric layer of copper wire (screen) which act as a protective earth (PE). It has four stranded aluminum conductor which are circular shaped with a cross-sectional area of 16mm^2 and cross-linked polyethylene (XLPE-chemical) insulation. The colours of the conductors are in accordance with HD: 308 and the cable are rated with a nominal voltage of 1 kV.

Figure 3.2. Structure of AXMK low voltage power cable [29]

Table 3.1. Physical and Electrical characteristics of some LV cables according to the manufacturer [27] [28] [29].

PHYSICAL CHARACTERISTICS OF THE CABLES				
Cable Type	Cores	Conductor cross-section [mm²]	Insulation	Outer sheath
AMCMK	4	20	Lead-free PVC	Lead-free PVC
AMCMK	3+concentric PE conductor	16	PVC	PVC
AMCMK	4		PVC	PVC
AXMK	4	16	XLPE(chemical)	PVC

ELECTRICAL CHARACTERISTICS OF THE CABLES.			
Cable Type	DC Resistance off phase conductor [Ω/km]	Operating Capacitance per core [pF/m]	Operating Inductance per core [nH/m]
AMCMK	1.83	400	280
AMCMK	1.91	400	260
AMCMK	0.868	450	270
AXMK	1.91	100	230

4 Input Impedance Measurements

The input impedance measurements were first performed on a healthy cable segment (AMCMK 3-phase) of 50m in length in order to characterize the cable by determining its parameters base on the impedance analysis at a high-frequency range (100 kHz–100 MHz). These measurements were all done offline. After the measurements have been performed on the healthy cable, various kinds of insulation degradation were performed on the cable and their respective cable input impedance were measured. The insulation degradations were performed at 17 m from the cable end port 0 (P0) as can be seen in figure 4.1.

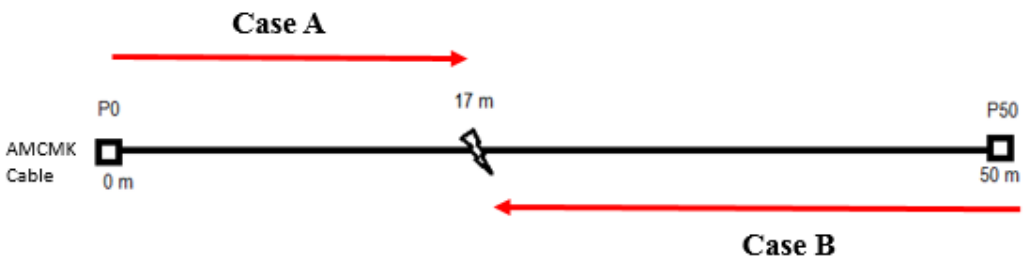

Figure 4.1. Studied underground LV cable ports configuration with the fault placed before the middle point (17 m from P0).

4.1 Input Impedance Measurement Setup

Input impedance measurements were performed using Hewlett-Packard Impedance Analyser 4194A (see appendix 2 Figure 2) with an impedance probe kit HP 41941A in the 100 kHz–100 MHz frequency range. The following cable conductors were measured: phase to phase measurements that involves L1, L2 coupling, and phase to ground measurement that involves L1, PE coupling. The measurements descriptions for both healthy cable and the faulty cable can be found in Table 4.1 and 4.2 respectively.

4.2 Effect of Distributed Parameters on Input Impedance Response

In order to have an in-depth knowledge about input impedance response of the AMCMK underground low voltage cable, the effect of the distributed parameters (r, l, g, and c) on the input impedance response were investigated using an algorithm based on transmission line theory (Appendix 1, figure 3). The values of the

parameters used in this investigation were extracted from input impedance measurements of the AMCMK cable within the frequency band of 100 kHz–100 MHz. The following conclusions were then drawn:

Input Impedance Response for Open-Circuit Cable Ends

- The increase in the distributed capacitance moves the impedance spectrum position downwards towards the negative vertical axis and decreases the amplitude of the spikes and vice versa.
- The increase in the distributed inductance moves the impedance spectrum position upwards towards the positive vertical axis and increases the amplitude of the spikes and vice versa.
- The increase in the distributed resistance moves the impedance spectrum position upwards towards the positive vertical axis and increases the amplitude of the spikes and vice versa.
- The increase in the distributed conductance moves the impedance spectrum position downwards towards the negative vertical axis and decreases the amplitude of the spikes and vice versa.

Input Impedance Response for Short-Circuit Cable Ends

- The increase in the distributed capacitance moves the impedance spectrum position downwards towards the negative vertical axis and decreases the amplitude of the spikes and vice versa.
- The increase in the distributed inductance moves the impedance spectrum position upwards towards the positive vertical axis and increases the amplitude of the spikes and vice versa.
- The increase in the distributed resistance moves the impedance spectrum position upwards towards the positive vertical axis and increases the amplitude of the spikes and vice versa.
- The increase in the distributed conductance moves the impedance spectrum position downwards towards the negative vertical axis and decreases the amplitude of the spikes and vice versa.

The above outcomes show that the input impedance response for both short and open-circuit cases are affected by the distributed parameters.

4.3 Input-Impedance Analysis

In order to understand the changes in the healthy cable characteristics as a result of the various damages inflicted on it, a comparison was drawn between the healthy cable and the faulty cable spectra as it can be observed in figure 4.2. According to Figure 4.3 (a), within the frequency band of 100 kHz–30 MHz, the input impedance spectra of all the open-circuit healthy and faulty cable with phase-to-phase (L1, L2) coupling as described in Table 4.1 exhibit much similarities with almost the same amplitude as depicted in their spectra spikes. As the frequency increases, the spectra start to exhibit very visible differences in their input impedance responses within the bandwidth of 30–60 MHz as shown in Figure 4.3 (b). The possible reason might be due to multiple reflections and power loss caused by the impedance discontinuity at the fault location [10]. However, in the same frequency range 30–60 MHz, it can also be seen that, the input-impedance spectra for the cable submerged in water for 18 hours that contains salt and the one without salt for 17 hours showed lots of similarities. The reason being that, they all have the same degree of damaged done to them and depending on how salty the water containing the salt is, both spectra could be similar or show some differences in their input impedance spectra. Besides that, both cables spent almost the same time in the water which might not add any significant difference between the spectra. The input impedance spectra for the other faults were quite different. The cable with 1st degree fault (shield removed) and was in the water for 30 hours (see Table 4.1) shows lower spikes compared to those with 2nd degree fault. The input impedance spectra for the fault measured from the other end of the cable; P50 **Case B** (Figure 4.1) exhibits very low amplitude in its input impedance spectrum. This could be due to the complex structure of the PVC insulation of the cable. The behavior of all the input impedance spectra at a frequency higher than 60 MHz is unpredictable and the reason is not known but most probably attributed to measuring devices.

Table 4.1. Measurement description of all healthy cable situation.

MEASUREMENTS DESCRIPTION		
Stages	Description	Hours in water
AMCMK_healthy_L1L2_oc	Healthy cable with phase to phase (L1, L2) open ends.	Dry
AMCMK_healthy_L1L2_ss	Healthy cable with phase to phase (L1, L2) short ends.	Dry
AMCMK_healthy_L1PE_oc	Healthy cable with phase to ground (L1,PE) open ends	Dry
AMCMK_healthy_L1PE_ss	Healthy cable with phase to ground (L1,PE) open ends	Dry

Table 4.2 Measurements description of all faulty cable situation where Case A represent measurements 17 m from P0 while Case B represent measurements 33 m from P50, thus the other end of the cable (Figure 4.1)

MEASUREMENTS DESCRIPTION		
Stages	Description	Hours in water
AMCMK_2dgf_17h_L1L2_oc	Cable with phase to phase (L1, L2) open ends and 2nd degree fault; damage (cut) to the outer sheath and the conductor insulation. Case A	17h
AMCMK_2dgf_17h_L1L2_ss	Cable with phase to phase (L1, L2) short ends and 2nd degree fault; damage (cut) to the outer sheath and the conductor insulation. Case A	17h
AMCMK_2dgf_17h_L1PE_oc	Cable with phase to ground (L1, PE) open ends and 2nd degree fault; damage (cut) to the outer sheath and the conductor insulation. Case A	17h
AMCMK_2dgf_17h_L1PE_ss	Cable with phase to ground (L1, PE) open ends and 2nd degree fault; damage (cut) to the outer sheath and the conductor insulation. Case A	17h
AMCMK_2dgf_17h_L1L2_oc_50_0	Cable with phase to phase (L1, L2) open ends and 2nd degree fault; damage (cut) to the outer sheath and the conductor insulation. Measurement taken from the 50m end of the cable. Case B	17h
AMCMK_2dgf_salty_18h_L1L2_oc	Cable with phase to phase (L1, L2) open ends and 2nd degree fault; damage (cut) to the outer sheath and the conductor insulation. Case A	18h
AMCMK_1dgf_30h_L1L2_oc	Cable with phase to phase (L1, L2) open ends and 1st degree fault; damage (cut) to the outer sheath. Case A	30h

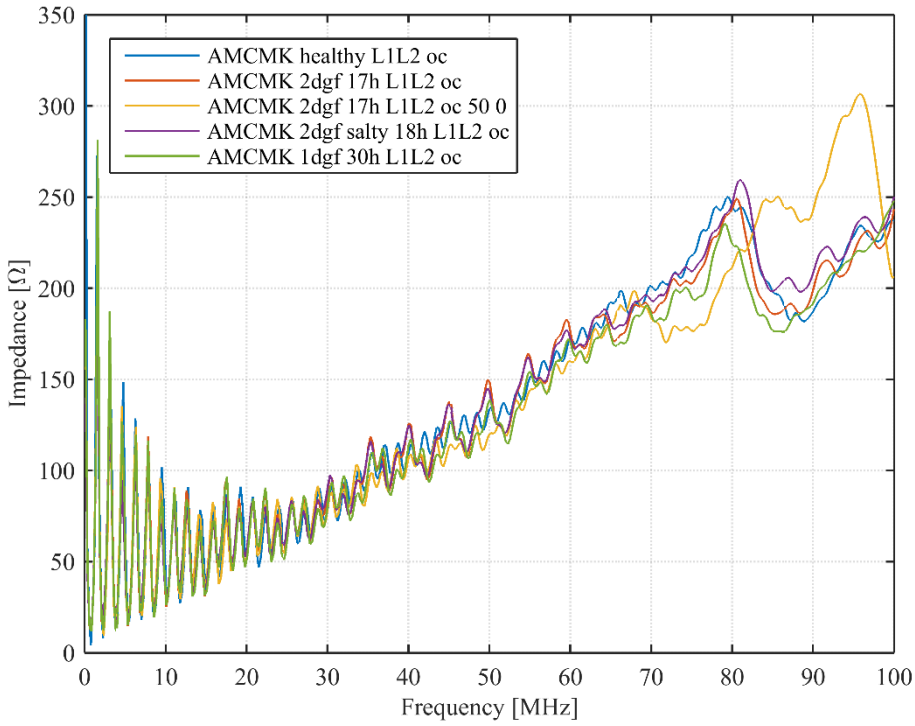

Figure 4.2. Input-impedance measurements spectra of all phase to phase (L1, L2) healthy and faulty AMCMK cable in an open-circuit situation between frequency bands of 100 kHz–100 MHz

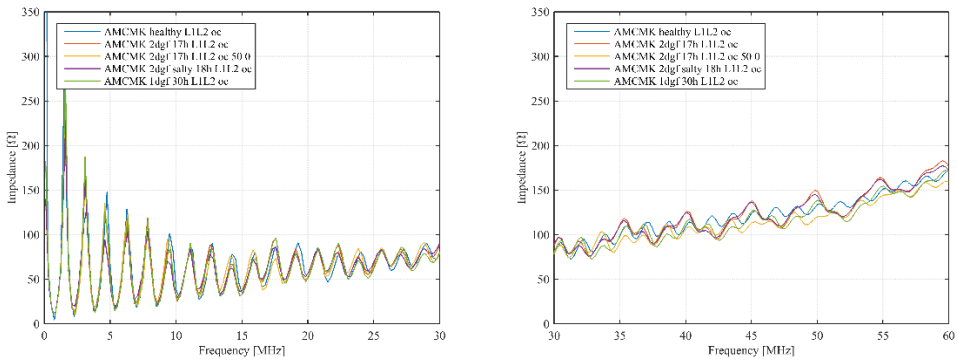

(a) (b)

Figure 4.3. Input-impedance measurements spectra of all phase to phase (L1, L2) healthy and faulty AMCMK cable in an open circuit situation between frequency bands of (a) 100 kHz–30 MHz (b) 30–60 MHz.

Figure 4.4 (a) and (b) illustrate the input impedance spectra of phase-to-ground (L1, PE) coupling for both healthy and faulty cable in an open circuit situation. As

the figure shows, both input impedance spectra match-up well within the frequency band 100 kHz–25 MHz but shows visible differences at the frequency higher than 25 MHz. The difference in the spectra is due to multiple reflections caused by the impedance discontinuity in the faulty cable. Moreover, it can also be observed that right from the 100 kHz–100 MHz both heathy and faulty cable input impedance spectra shows inconsistency in the amplitude of their spikes as the signals attenuate. The nature of the wave is as a result of the coupling effect of the other two conductors which were not used in the measurements since the AMCMK cable is a multi-conductor cable. The coupling effect is possibly caused by an uneven capacitance and inductance that exist between the conductor of the cable used in the measurements and the ground and that of the other two conductors and the ground from the point of measurements.

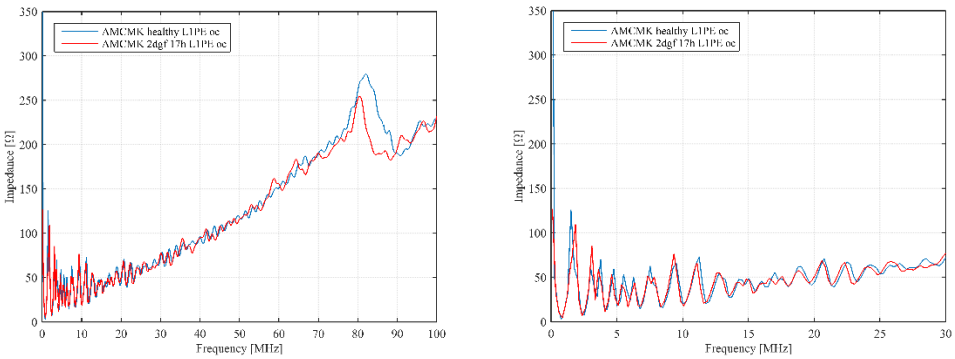

Figure 4.4. Input-impedance measurements spectra of phase-to-ground (L1, PE) healthy and faulty AMCMK cable in an open-circuit situation between frequencies band of (a) 100 kHz–100 MHz and (b) 100 kHz–30 MHz.

In the case of impedance measurements conducted on the AMCMK cable with phase-to-phase (L1, L2) coupling in a short-circuit scenario, the resulting input-impedance spectra are illustrated in Figure 4.5. As it can be seen, the input impedance spectra of the healthy and the faulty cables are quite similar within the frequency band 100 kHz and 30 MHz. As the frequency increases above 30 MHz, the spectra reveals very visible differences due to multiple reflections that occur at the boundary of impedance discontinuity caused by the damage inflicted on the sheath and the conductor insulation.

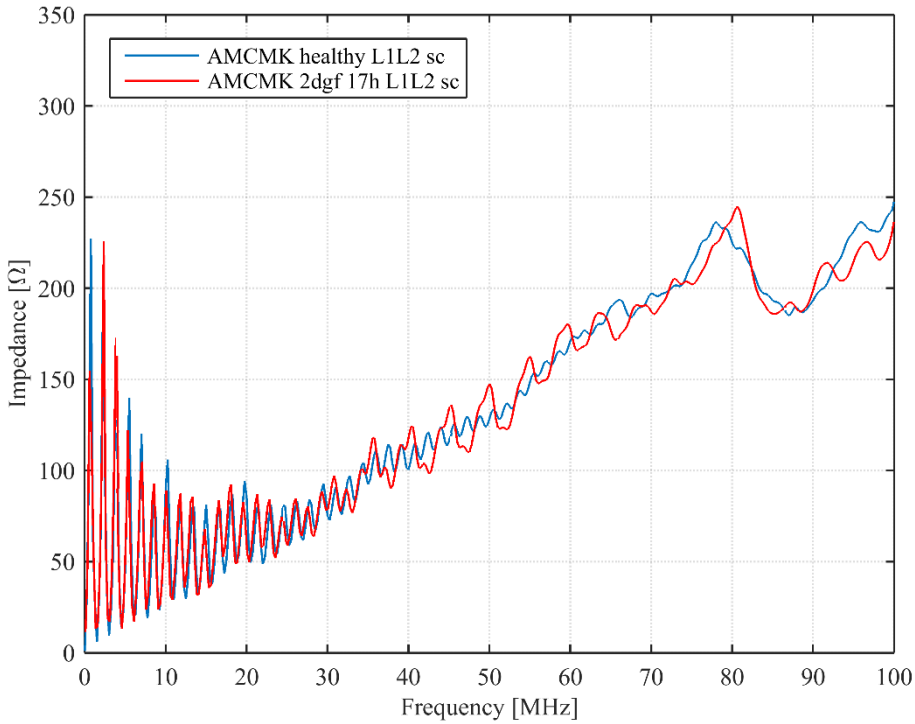

Figure 4.5. Input-impedance measurements spectra of phase-to-phase (L1, L2) healthy and faulty AMCMK cable in a short-circuit situation between frequency band of 100 kHz–100 MHz

Input impedance spectra of healthy and the faulty cable in phase to ground (L1, PE) coupling when the cable is short circuited is illustrated in Figure 4.6. As shown in the figure, the spectra for the healthy and the faulty cable can be seen to be visually similar within the frequency band of 100 kHz and 32 MHz. At higher frequency above 33 MHz the differences in the spectra is seen to become visible. The possible reason is that the fault in the cable causes high impedance boundary which starts to reflect part of the propagating signal. The cause of bias and the steep notch in both signal is not known but most probably attributed to the instruments used to perform the measurements.

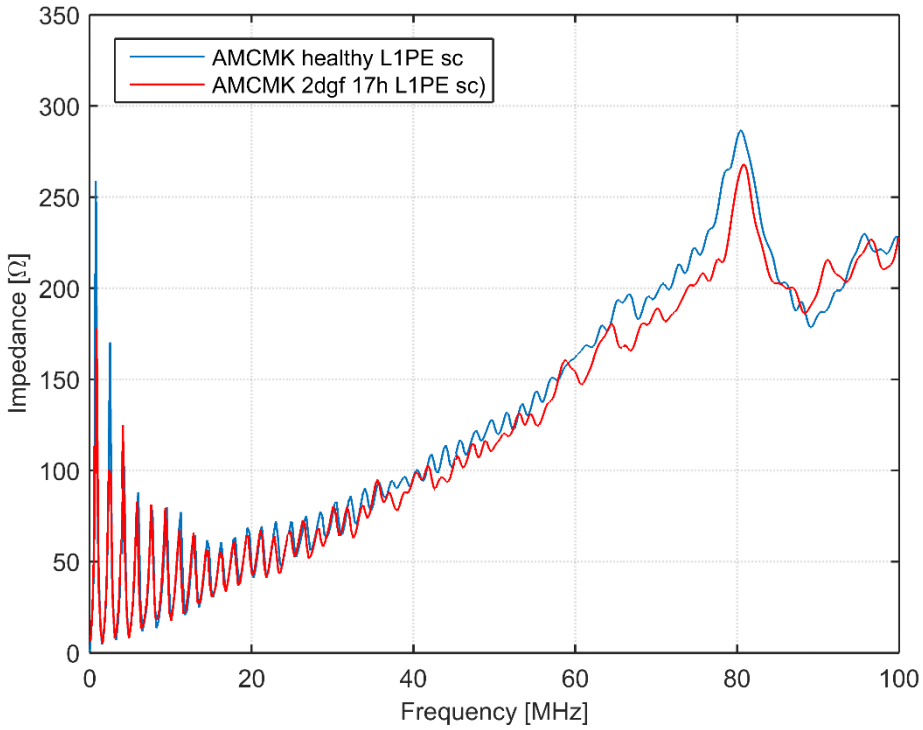

Figure 4.6. Input-impedance measurements spectra of phase-to-ground (L1, PE) healthy and faulty AMCMK cable in a short-circuit situation within the frequency band of 100 kHz–100 MHz.

5 Modeling of Power Cable - State of the Arts

Modeling of a power cable has been an area of study interests in recent times as it can be applied to evaluate the power line communication (PLC) channel. This is practically based on the same principle as PLC channel modeling. There are many developed different approaches that are used to model the PLC channel, among them, are multipath study through GEESE algorithm [30], one-parameter deterministic model [31], wavelet-based [32], the use of competitive neural network [33] etc. In practice, all the approaches are categorized into the top-down approach and bottom-up approach [9]. The latter is further divided into the two-conductor transmission line model and multi-conductor transmission line model. There are also future works such as random channel generation, channel model generalization and channel modelling for smart grid communication systems being developed according to [9].

5.1 Top-Down Approach

The top-down approach utilizes data fitting technique to derive the most fitted model from measurements, which may either result from the frequency or impulse response. According to [9], this approach treats the PLC channel as a black box, excites it with a reference signal in either frequency or time domain and as a result a large number of measurement is collected and by applying a complex fitting algorithm, a model that fit the measurements is found. The approach intends to utilize not many cable parameters to approximate the channel with high accuracy. The advantage of this method is that the generated model is easy to use and allows fast channel generation making it suitable for a simulation where a wide channel that consists of cables connected together is needed. The disadvantageous aspect of this approach is its low flexibility as different networks and frequency bands that need to have their own model. Detailed explanation and example of modelling approach can be found in [9] where for instance details about a multipath phenomenon can be found.

5.2 Bottom-Up Approach

The transmission line theory which describes how electromagnetic wave propagates in a transmission line as explained in Chapter 2 is based on this approach. However, the theory alone is not very useful unless it is modified or applied with other methods such as the voltage ratio approach, the ABCD matrix and S-parameters before it can be utilized to model signal propagation in the network. The latter uses transmission and reflection coefficients to describe wave propagation. The ABCD matrix and the voltage ratio rely on the voltages and the currents at network nodes and that makes it useful in a situation where there are different number of conductors connected together [9]. The advantage of this approach is its flexibility to cope with the various situation so long as the information about the network (topology, parameter, loads etc.) is well known. This has a close relationship with the power network since it is derived from the physical interpretation of electromagnetic wave propagation in transmission line network making it suitable for network-related system modelling. However, it suffers from several drawbacks, which includes computational complexity. Practically, this method is not probably a good option as it only considers several elements of the network. According to [34], a great number of parameters cannot be determined with sufficient precision in this approach. The practical model must take into account many other natural and artificial interferences like weather and radio signals. Also collection of network information previously indicated becomes challenging due to their large number of variation. [9]

The bottom-up approach is subdivided into two-conductor line model and multi-conductor model theory. The two conductor theory is used for power network connected with the two-conductor transmission line while the multi-conductive theory is applied to the transmission line with more than two conductors as can be found in [9].

5.3 Theory of Broadband Impedance Spectroscopy

Broadband impedance spectroscopy (BIS) is novel approach for diagnosis, prognosis and estimating faults location in a cable which is based on the measurement

of broadband impedance response of the power cable [12]. BIS measures the magnitude of the cable impedance as a function of a wide range of frequency [35]. The method which employs transmission line theory has several merits. According to [12], impedance response of the power cable is affected by both the cable insulation material and the fault. Secondly, the scanning range can be adjusted by the selection of a frequency band. Lastly, the method could be integrated as a software algorithm to modern broadband power line communication modems which use orthogonal frequency-division and multiplexing (OFDM) [36] as a channel access method. OFDM has high bit-rate transmission over frequency-selective and time-variant channels [33], high spectral efficiency, simple implementation, and robustness to frequency-selective distortions [37].

The theory of BIS is based on transmission line theory. The input impedance of both open and short circuit is given by (5.1) and (5.2), respectively.

$$\mathbf{Z}_{\text{cable,oc}}(\omega) = \mathbf{Z}_0(\omega)\coth[\boldsymbol{\gamma}(\omega)L], \tag{5.1}$$

$$\mathbf{Z}_{\text{cable,sc}}(\omega) = \mathbf{Z}_0(\omega)\tanh[\boldsymbol{\gamma}(\omega)L]. \tag{5.2}$$

where L is the length of the cable. From both (5.1) and (5.2), it can be seen that the input impedance is a function of frequency. Figure 5.1 illustrates an equivalent circuit for open-ended cable situation. Some of the incident signal are reflected by the fault impedance ($\mathbf{Z_f}$). The reflected signal travels back to the source and the rest goes through where it is reflected back from the high impedance open ends.

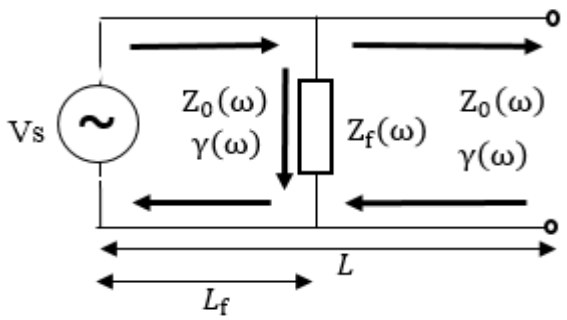

Figure 5.1. Open-ended cable with a phase-to-phase fault. Reflected and propagating currents are marked into the figure with arrows. L_f denotes distance from the source at which the fault occurred.

The input impedance for the cable segment from the fault location to the cable end is given by

$$\mathbf{Z}_{\text{cable,oc}}(\omega) = \mathbf{Z}_0(\omega)\coth[\boldsymbol{\gamma}(\omega)(L - L_{\text{f}}], \tag{5.3}$$

The total load impedance $\mathbf{Z}_{\text{Load}}$ at the location of the cable fault is presented with parallel connection of (5.3) and the fault impedance $\mathbf{Z}_{\text{f}}$ as expressed in (5.4).

$$\mathbf{Z}_{\text{load}}(\omega) = \frac{\mathbf{Z}_{\text{cable,oc}}(\omega)\mathbf{Z}_f(\omega)}{\mathbf{Z}_{\text{cable,oc}}(\omega)+\mathbf{Z}_f(\omega)}. \tag{5.4}$$

Finally, the total system input impedance at the signal source is

$$\mathbf{Z}_{\text{in}}(\omega) = \frac{\mathbf{Z}_{\text{Load}}(\omega) + \mathbf{Z}_0(\omega)\tanh[\boldsymbol{\gamma}(\omega)L_f]}{\mathbf{Z}_0(\omega)+\mathbf{Z}_{\text{Load}}(\omega)\tanh[\boldsymbol{\gamma}(\omega)L_f]}. \tag{5.5}$$

6 Modeling of AMCMK Power Cable

The modeling basis on a 50 m long AMCMK power cable used in the measurements. In order to model the AMCMK cable, the lumped model for healthy cable is first designed. The parameters for the cable model are estimated and tuned through input impedance measurements performed on the AMCMK cable for various signal coupling as listed in Table 6.1. The instruments used in performing the impedance measurement is an HP4194A impedance analyser with an HP41941A impedance probe kit as shown in Appendix II Figure 3.The models for the various faults under consideration are inserted into the cable model at the point where the failure occurred. Thus the point 17 m from the signal source or the measurement point P0 (see Figure in 4.1). The parameters used in tuning the fault models are listed in Table 6.2.

6.1 Model for Healthy Cable

There are two cases for the cable model; the model for a short circuit case (Figure 6.1. a) and an open circuit case (Figure 6.2. (a)). The algorithm for the models was based on BIS (Chapter 5.3) and on the transmission chain parameter matrix theory as explained in Chapter 2.4. In the open circuit situation, $\mathbf{Z}_{load}$ is assumed to have high value since there is no conduction path to the load as it can be seen in the algorithm in Appendix I Figure 1. The input impedance of the cable is then calculated by applying (5.5). Accordingly, the input impedance of the short-circuit case is calculated but $\mathbf{Z}_{load}$ is presumed to be zero ($\mathbf{Z}l_{oad} = 0$) as the phases (L1, L2 or L1, PE coupling) are short-circuited.

Table 6.1. Parameters used in modelling the healthy 50 m AMCMK low-voltage cable, where $Z_0(\Omega)$ is the characteristic impedance, v_p/c_0 is the velocity of the propagation, $l(\mathrm{nH/m})$, c $(\mathrm{pF/m})$ and $r(\Omega)$ are the distributed inductance, capacitance, and resistance, respectively with signal coupling phase-phase (L1, L2) and phase to ground (L1, PE). Conductance is not included in the model since it is a function of the distributed capacitance and the frequency of the source signal.

Cable end Open-Circuited (Healthy Cable)					
Signal Coupling	$Z_0(\Omega)$	v_p/c_0	$l(\mathrm{nH/m})$	c $(\mathrm{pF/m})$	$r(\Omega)$
L1, L2	42	0.535	249	138	1.6
L1, PE	25	0.530	249	138	1.6
Cable end Short-Circuit (Healthy Cable)					
L1, L2	42	0.520	249	138	1.6
L1, PE	25	0.570	249	138	1.6

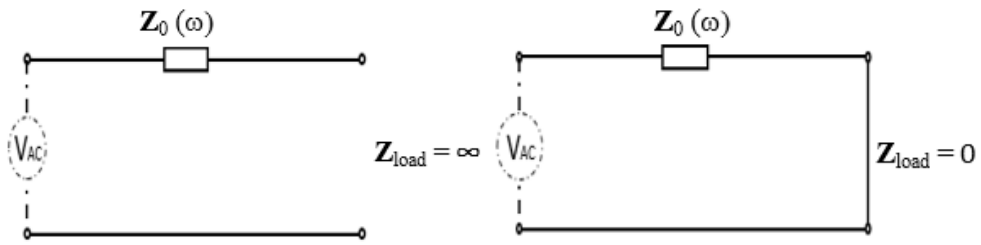

(a) (b)

Figure.6.1. Cable model (a) open-circuit (b) short-circuit cable (healthy).

The input impedance spectra for both model and measurements of the healthy cable in an open-circuit case for signal coupling between L1, L2 and L1, PE in this study are illustrated in Figures 6.2 and 6.3 respectively. In the spectra for L1, L2 coupling, the magnitude of the both model and the measurements are similar between the frequency band of 100 kHz and 50 MHz. As it can be seen in the spectra, there is distortion in measurements spectrum between the frequency bands of 50–100 MHz. The reason might be due to inconsistency in the physical property structure of the PVC insulation of the cable as explained in [10]. The reason for the bias seen in the spectra is not really known but could be attributed to the inaccuracy in the measuring instrument as the same phenomenon exhibits in all the spectra for the various couplings under consideration in this study.

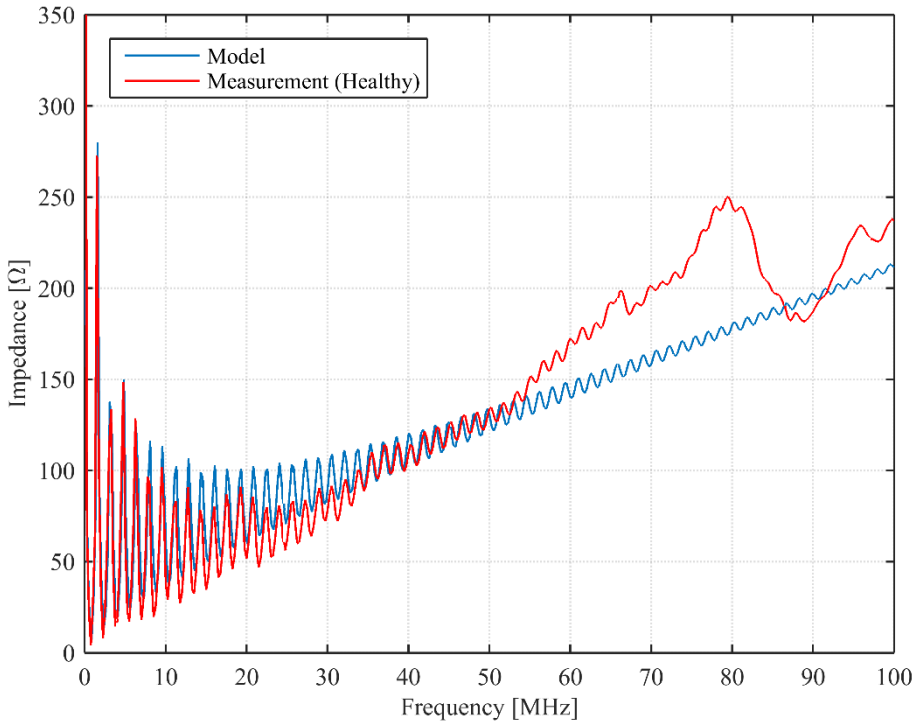

Figure 6.2. Measured and modeled input impedances of phase-to-phase (L1, L2) healthy AMCMK cable in an open circuit situation in the frequency band between 100 kHz–100 MHz

In the case of L1, PE coupling, as it can be seen in Figure 6.3, the measurements and the developed model spectrum are visually similar within the frequency band of 100 kHz–20 MHz except for the fact that the amplitude of the spikes in the measurements spectrum has reduced. The reduction in the amplitude of the spike in the measurements spectrum can further be seen between the frequency bands 20–100 MHz. In the same band (20–100 MHz) the measurement spectrum exhibit distortion in the wave. The reason for the reduction and the distortion in the measurements spectra is due to additional capacitance and inductance between the L1 and the other two phases (L2, L3), which have an effect on the measurements since the LV AMCMK cable is a multi-conductor cable.

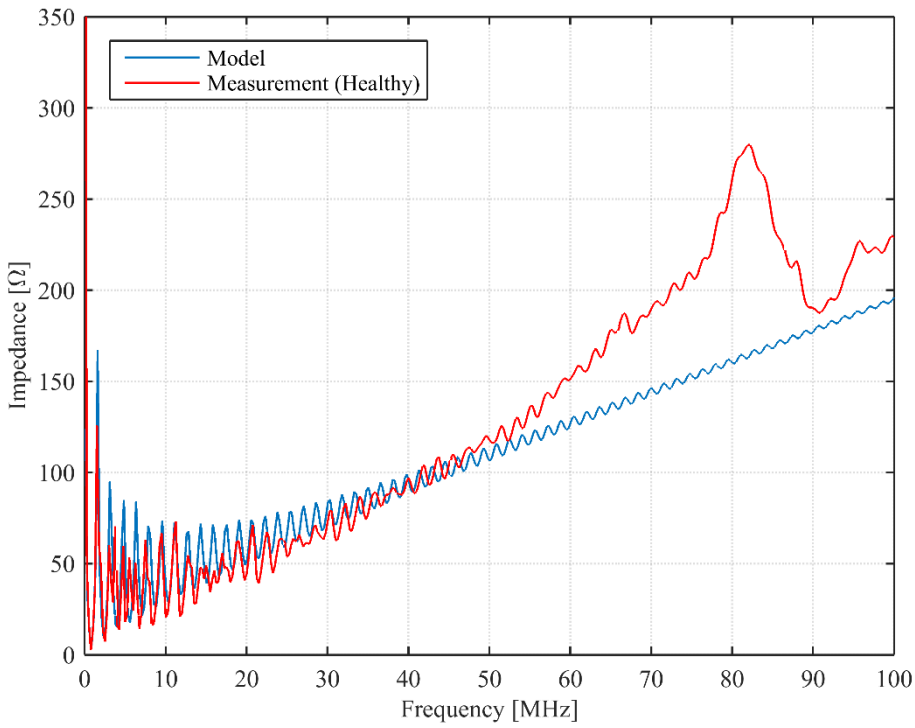

Figure 6.3. Measured and modeled input impedances of phase-to-ground (L1, PE) healthy AMCMK cable in an open-circuit in the frequency band between 100 kHz–100 MHz.

Figures 6.4 and 6.5 illustrate input impedance spectra for the phase to phase (L1, L2) and phase to ground (L1, PE) coupling in a short-circuit case. As seen in Figure 6.4, the measurements and the cable model spectra are visually similar, exhibiting similar spikes. Like in the open-circuit case, the measurement spectrum starts to exhibit some kind of bias and a wave pattern, which are far from the developed model spectrum within the frequency band of 52–100 MHz. The reason is what has been mentioned earlier on, that it might be from the instruments used in the measurements.

In the L1, PE coupling for short-circuit case, the model, and the measurements spectra are more similar visually, compared to the open-circuit case as it can be seen in Figure 6.5. Though, there appears a phase shift between the measurements and the developed model spectra from 30 MHz as the model spectrum lags the measurements spectrum. The reason why the spectra more similar visually in L1, PE coupling in short-circuit case can be explained as the high conductive path

between the conductors L1, PE which reduce the effect of the coupling between the L1 and the other phases (L2 and L3) to course distortion in the measurements spectrum. The phase shift might be probably attributed to the inconsistency in the PVC insulation micro-structure.

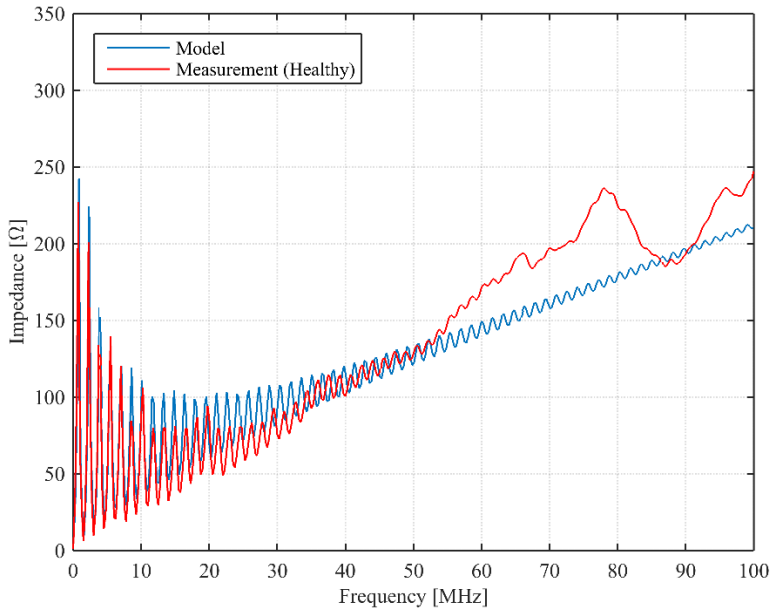

Figure 6.4. Measured and modeled input impedances of phase-to-phase (L1, L2) healthy AMCMK cable in a short-circuit case in frequency band of 100 kHz–100 MHz.

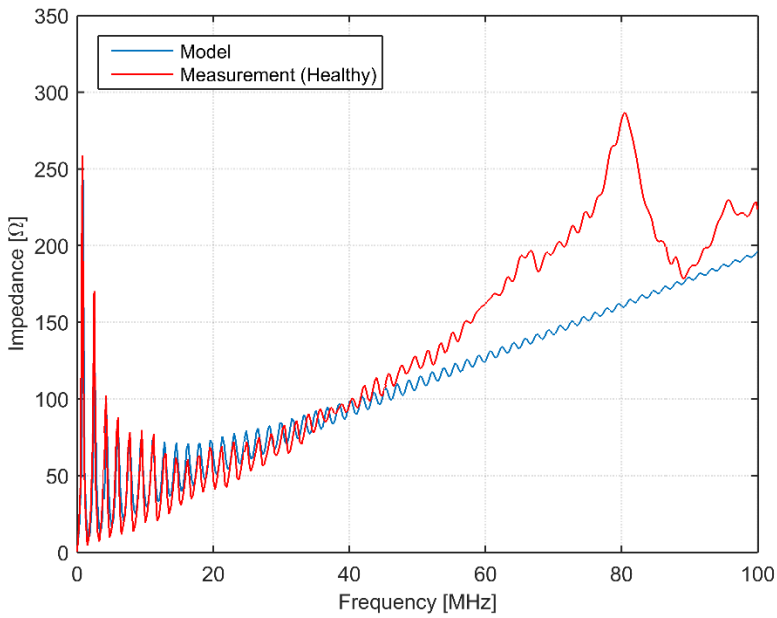

Figure 6.5. Measured and modeled input impedances of phase-to-ground (L1, PE) healthy AMCMK cable in a short-circuit situation at frequency band of 100 kHz–100 MHz.

6.1 Model for Faulty Cable

The various faults associated with this study are all modelled in this subsection. The models are developed for each coupling, thus L1, L2 and L1, PE in an open and short-circuit cases and are tuned for each specific fault separately. First, a common model for all the open-ended faults for L1, L2 coupling are developed and tuned for the various faults being considered in this study as listed in Table 4.2. This is followed by the model for LI, L2 coupling fault in a short-circuit case. Next, the model for both L1, PE open and short-circuit cases followed respectively.

6.1.1 *Model for Phase to Phase Open Circuit Faults*

The model for open circuit L1, L2 coupling consists of a shunt capacitor and an inductor connected in series. Thus, a series resonance circuit is connected parallel to the very high load impedance as it can be seen in Figure 6.6. In the cable fault algorithm, which can be found in Appendix I (Figure 1), the fault model matrix is cascaded (see figure 2.6 and (2.22)) with the healthy cable model matrices by inserting it at the point 17 meters from the measurement point P0 according to Case A (see Figure 4.1) to simulate the measured fault signature. By varying the fault modeled parameters (shunt capacitance and the inductance), a match-up spectra of the modelled and the measurements are achieved. The values used for the fault model capacitance and the inductance are listed in Table 6.2. These values are found by tuning the model parameters during the simulation in the Matlab environment.

Table 6.2. Parameters used for modelling all the faults under consideration in 50m AMCMK low-voltage cable, where $l(\mathrm{nH/m})$, c $(\mathrm{pF/m})$ and $r(\Omega)$ are the distributed inductance, capacitance and resistance, respectively, for the signal coupling phase-phase (L1, L2) and phase to ground (L1, PE).

Open-Circuit (Fault)			
Signal Coupling	$l(\mathrm{nH/m})$	c $(\mathrm{pF/m})$	$r(\Omega)$
L1,L2 (17hrs)	49.80	92.00	
L1,L2 (17hrs)_50	199.2	92.00	
L1,L2 (18hrs)_Salty	49.80	55.20	
L1,L2 (30hrs)_1st deg.	49.80	39.43	
L1,PE(17hrs)	2.49	138.00	1.6
Short-Circuit (Fault)			
L1,L2 (17hrs)	87.15		16
L1,PE (17hrs)	49.80		1.6

The resulting input impedance spectra for both measured and modelled case are illustrated in Figure 6.7. As it can be seen the input impedance spectra for the modelled visually follows the measured input impedance except for the bias in the measurements spectrum, which might be attributed to the measuring instrument.

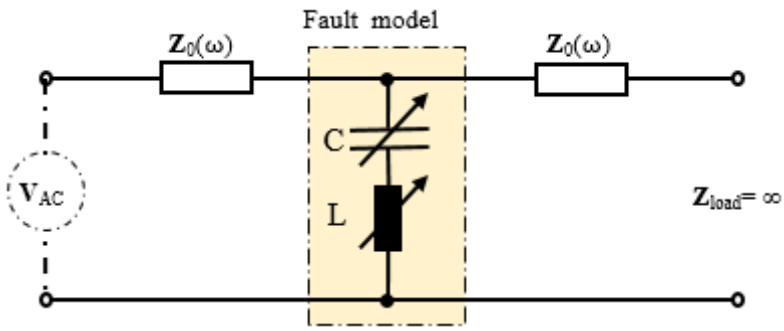

Figure 6.6. Two-port input impedance model for simulation of open-circuit L1, L2 cable fault. The fault model is inserted in-between the cable where the fault occurred, thus 17 meters from the signal source.

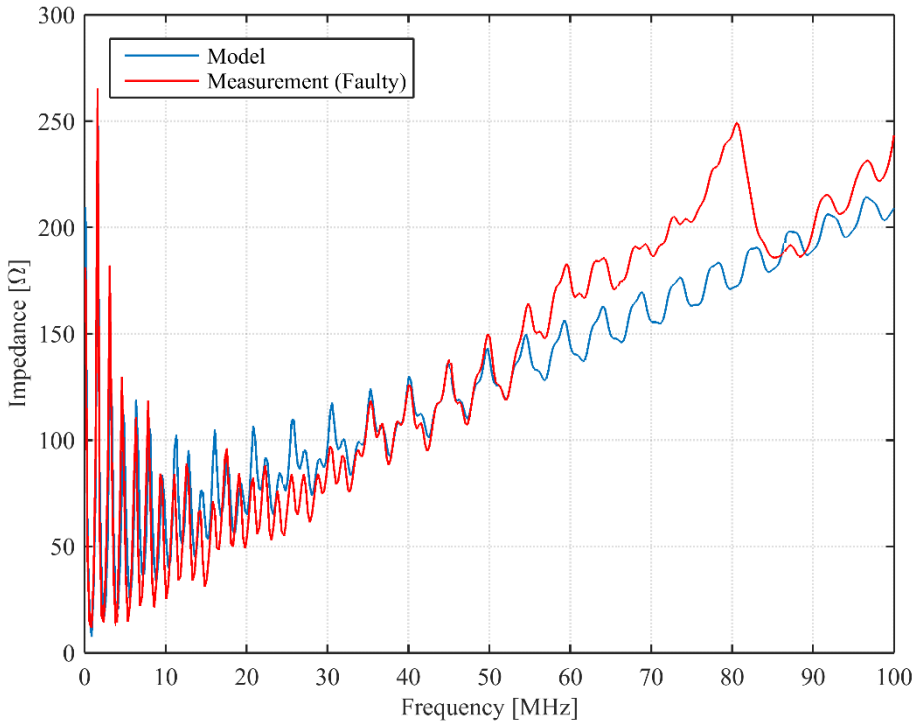

Figure 6.7. Measured and modeled input impedances of phase-to-phase (L1, L2) coupling of a faulty AMCMK cable in an open circuit situation in frequencies band between 100 kHz–100 MHz (**Case A**).

In Figure 6.8, the measured and the modeled spectra in **Case B** situation (see Figure 4.1) are visually closed within the frequency band of 100 kHz–15 MHz. Between the frequency band of 15 MHz and 100 MHz, there is a small phase shift between the modeled and the measured spectra. The shift may be due to the complex micro-structure of the PVC insulation material of the cable. Again, from 67 MHz to 100 MHz the nature of the measurements spectra is difficult to describe but presumed to be coursed by the measuring instrument.

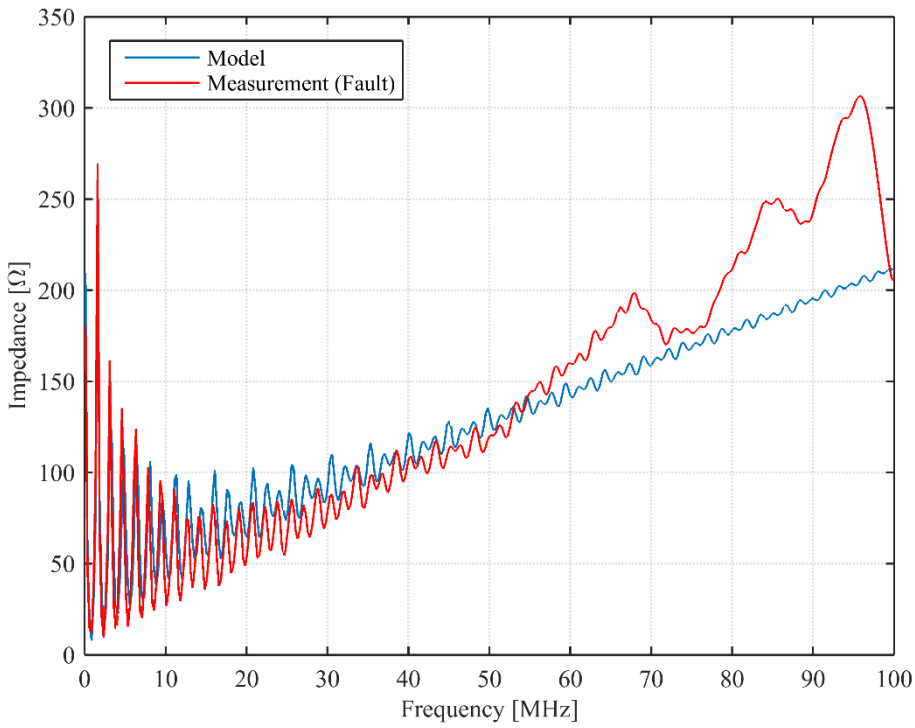

Figure 6.8. Measured and modeled input impedances spectra of phase-to-phase (L1, L2) Faulty AMCMK cable in an open-circuit situation between frequencies band of 100 kHz–100 MHz measured from the other end other cable (**Case B**).

Figure 6.9 illustrates the measured and the modeled input impedance spectra for the cable with 2nd degrees fault, thus, damage to both the shield and the conductor insulation and submerged in salty water for 18 hours. The tuning parameters can be found in Table 6.2 as well. Within the frequency band of 100 kHz–51 MHz, the modeled spectrum visually follows the measured spectrum, though the amplitude of the spikes for the measured spectrum is seen to be lower within the frequency band of 22–33 MHz. Between the frequency band of 50 MHz and 100 MHz, the modeled spectrum is seen to followed the measured spectrum only that the measured spectrum exhibits some notch between 75 MHz and 85 MHz.

Also in Table 6.2, the value of the capacitance used in tuning this fault model is seen smaller compared to the previous cases already explained. The reason might probably be the extra ions introduced into the water by the salt, which decreases the dielectric strength or increases conductivity between the two conductors (L1, L2). Salt (for example NaCl) in water forms delocalized sodium ions (Na^+) and

chlorine ions (Cl^-) i. Since the electric current flow is carried out by ions the presence of free ions in the water enhances conductivity between the conductors.

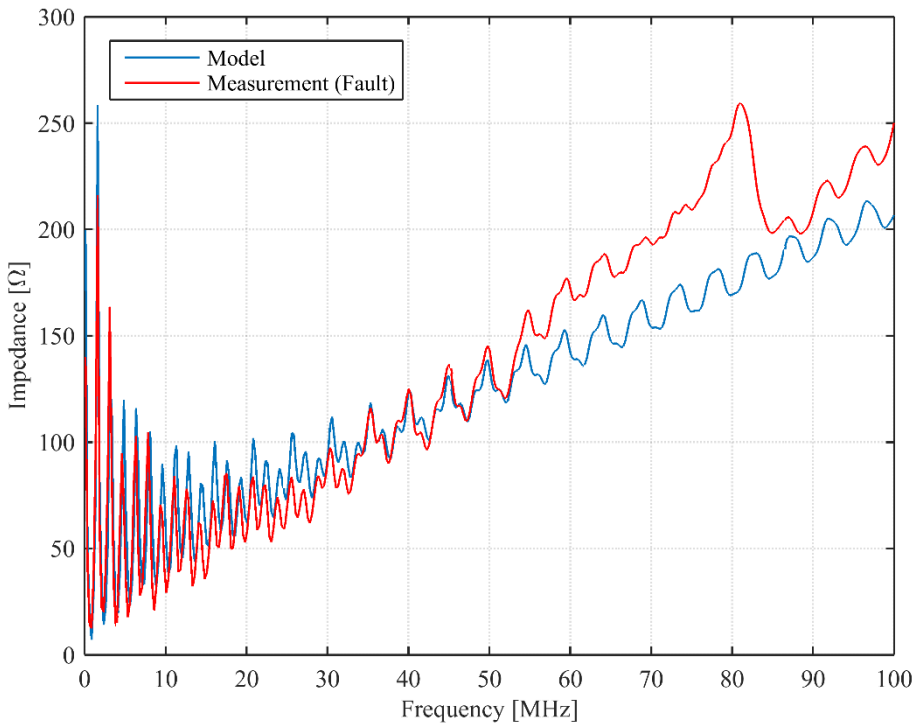

Figure 6.9. Measured and modeled input impedances spectra of phase-to-phase (L1, L2) faulty AMCMK cable in an open-circuit situation in the frequency band of 100 kHz–100 MHz. Cable with second degree fault immersed in salty water for 18 hours.

In Figure 6.10, the input impedance spectra of both measured and modelled spectra with 1st degree damage (sheath removed) to the cable and place in the water for 30 hours is illustrated. As it can be observed, the measured and the modeled spectrum are much closed. Just like all the figures in this Chapter, there is a bias after 50 MHz frequency. In the simulation, a low capacitive value for the fault is utilized compared to the other cases already discussed in this chapter as listed in Table 6.2. The possible reason is that the cable is left under the water for a long time (30 hours) and had more ingress of water in the insulation material, which creates a relatively high conductive path between the conductors.

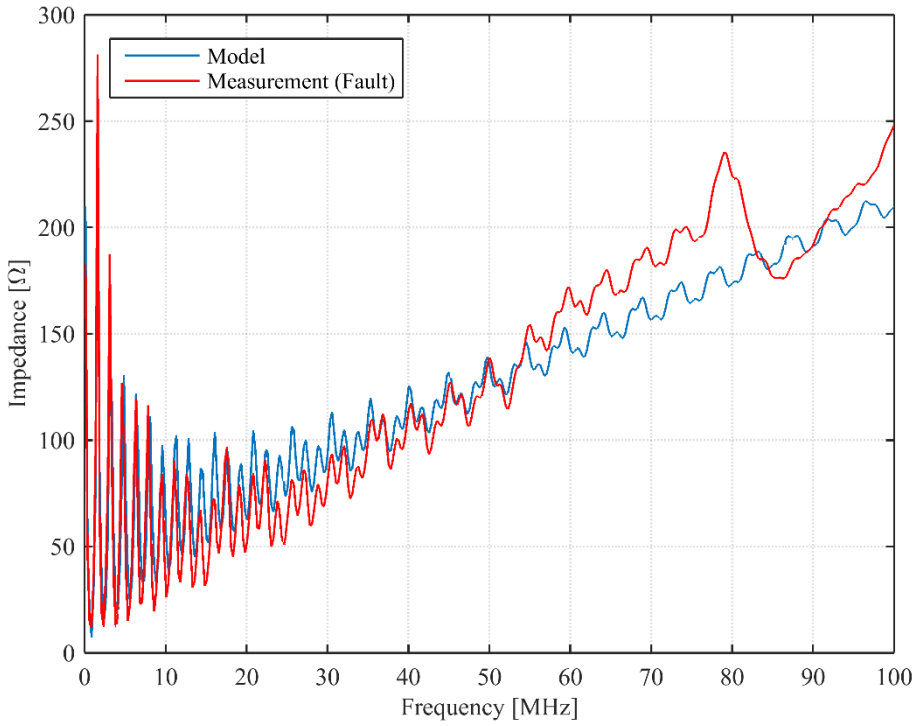

Figure 6.10. Measured and modeled input impedances spectra of phase-to-phase (L1, L2) faulty AMCMK cable in an open-circuit situation at frequency band 100 kHz–100 MHz. Cable with 1st degree fault and immense in salty water for 30 hours.

6.1.2 *Model for Phase to Phase Short Circuit Fault*

The simulation model for phase to phase (L1, L2) short circuit fault consists of series distributed resistance and inductance (R-L) circuit which are connected in series with the healthy conductors L1, L2 as it can be observed in Figure 6.11. A short-circuit between L1, L2 create a direct path for the current to flow from one conductor to the other. The R-L circuit was caused by the skin effect in the higher frequencies greater than 50–60 Hz. Skin effect is caused by the flow of AC current at the peripheral of a conductor instead of towards the center due to self-inductance within the conductor. As the frequency increases, the skin effect causes an increase in the cable resistance. In Table 6.2. The tuned values used in the simulation can be found. The value of the resistance used in the fault model could be seen higher compared with the one when there was no fault in the healthy cable. This fault model is a parameter adjustable as presented in Figure 6.11. It can be tuned to

generate a clear signature of the fault. The algorithm used in simulating this model can also be found in appendix I Figure 2.

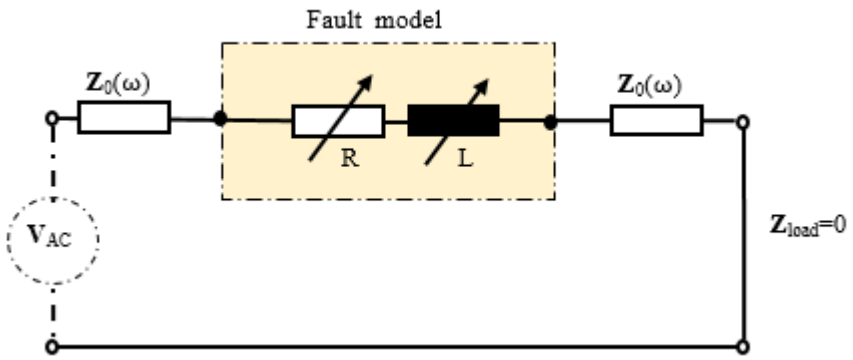

Figure 6.11. Developed two-port input impedance model for simulation of short-circuit phase to phase (L1, L2) cable fault, illustrating how the fault model is placed in the healthy cable.

The resulting input impedance spectra of both the measured and the modelled are shown in Figure 6.12. The spectra of the measurements and the modelled show a good match-up within the frequency band of 100 kHz–22 MHz. It can also be observed that, in the frequency band of 22–60 MHz both the modelled and the measured spectra are visually quite closed though there is a small phase shift between the spectra. In general, both spectra are visually closed. The evidence is visible even within the frequency band 90–100 MHz.

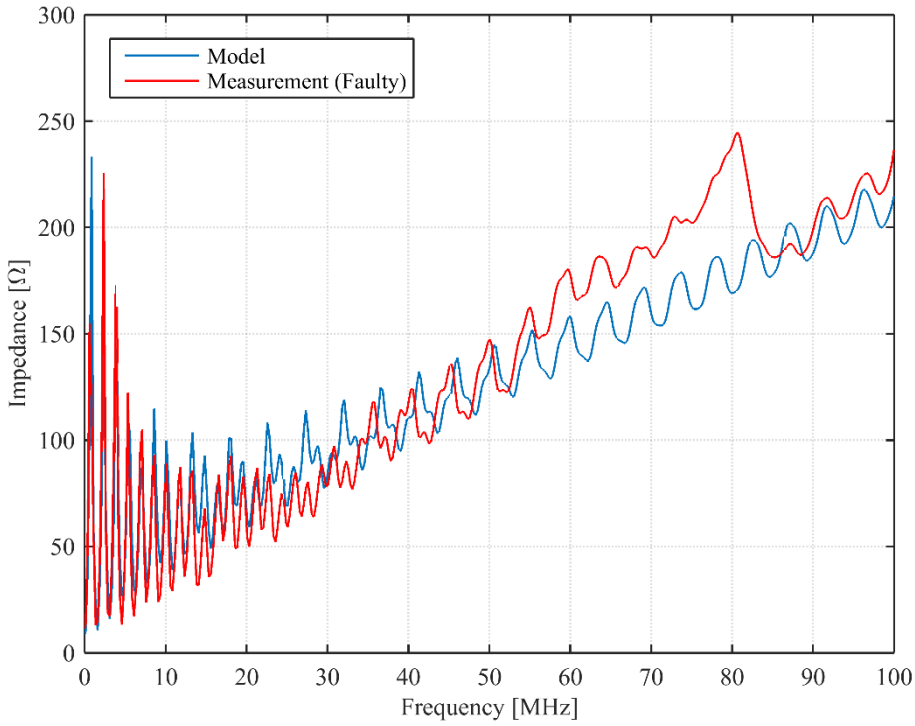

Figure 6.12. Input-impedance measurements and model spectra of phase-to-phase (L1, L2) coupling of faulty AMCMK cable in a short-circuit situation between frequency band of 100 kHz–100 MHz

6.1.3 *Model for Phase to Ground (L1, PE) Open-Circuit Fault*

Figure 6.13 illustrates the developed fault model used for simulating the open-circuit phase to ground fault between L1 and PE of the AMCMK cable. The Fault modelled consists of series RLC circuit, where *R*, *L*, and *C* denote resistance, inductance and capacitance, respectively. The fault is inserted in the cable model, thus, 17 m from the measurements point P0 (Appendix II Figure 4) where the fault is created and in parallel to the high load impedance as it is seen in Figure 6.13. In the algorithm, the fault is cascaded (see Figure 2.6 and (2.22)) with two parts of the healthy cable, thus at 17 m from the measurement point P0 and the rest of the 33m length of the cable. The values used in tuning the fault modelled can be found in Table 6.2 and the resulting simulated spectra can be found in Figure 6.14.

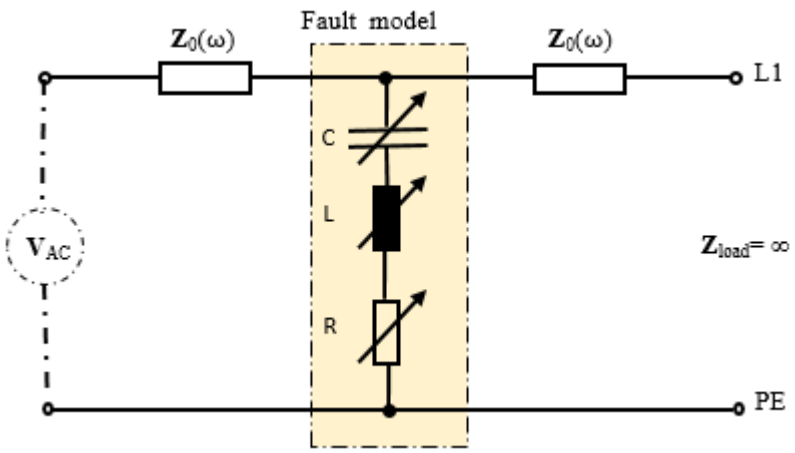

Figure 6.13. Developed two-port input impedance model for open circuit phase to ground (L1, PE) coupling fault.

Figures 6.14 illustrate the spectra of measured input impedance of AMCMK cable and the modelled faulty for L1, PE coupling. Within the frequency band of 100 kHz–13 MHz, it can be observed that the measured and the modelled spectra visually fit. This is not the case as the frequency increases especially within the frequency band of 13–55 MHz as the measured spectrum exhibits distortion and in the waveform. The possible reason could be attributed to a more complex structure of the faulty cable and the coupling effect of the other two cables, which are not used in the measurements. All the same, the model seems to work quite well as both spectra still show the same kind of waveform within the frequency band of 55–100 MHz when the bias and the notch within the range are ignored.

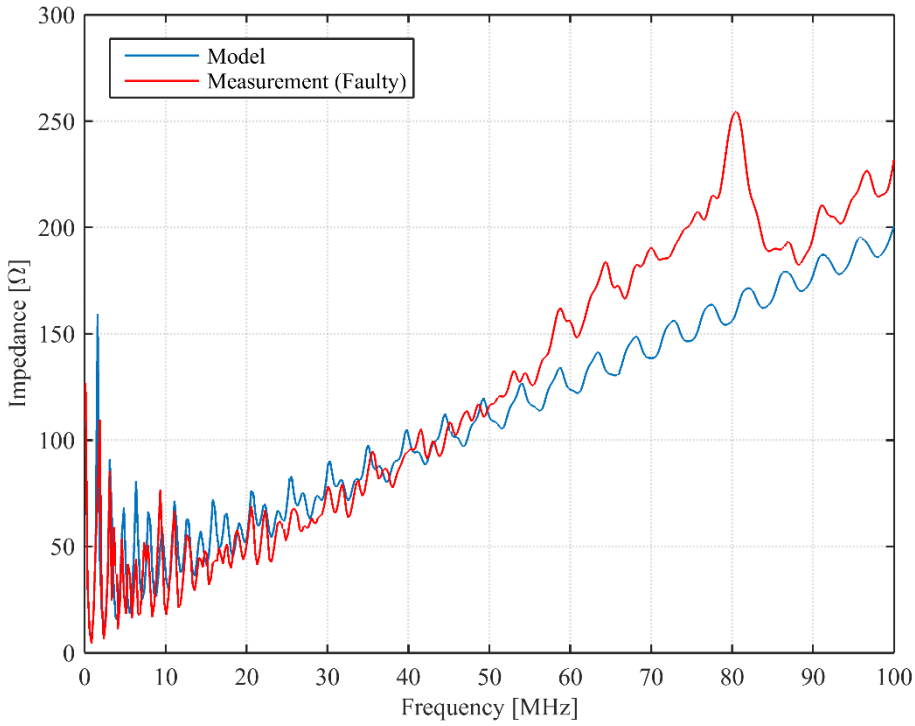

Figure 6.14. Measured and modeled input impedance spectra of phase-to-ground (L1, PE) coupling faulty AMCMK cable in an open circuit situation within the frequency band 100 kHz–100 MHz

6.1.4 *Model for Phase to Ground (L1, PE) Short-Circuit Fault*

Figure 6.15 illustrates the developed model for the phase-to-ground (L1, PE) short-circuit fault. The model consists of series distributed resistance and inductance (R-L circuit), which are connected in series to the conductors (L1, PE). A short-circuit between L1, PE creates a direct path for the current to flow from L1 conductor to the PE conductor. As explain in Chapter 6.1.2, the flow of ac current in a conductor causes skin effect as the frequency of the current increases above 50–60 Hz. This phenomenon increases the resistance of the conductor. The RL circuit of the conductor is tuned to achieved the short-circuit fault signature.

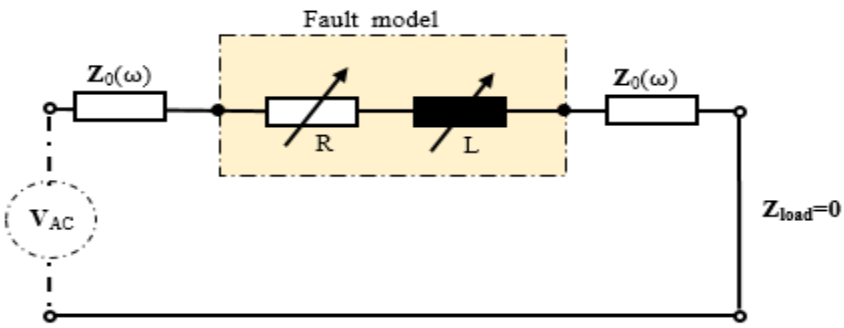

Figure 6.15. Developed two-port input impedance model for short–circuit L1, PE cable fault.

Figure 6.16 shows the corresponding measured input impedance and the modeled spectra. In the frequency band of 100 kHz–40 MHz the model and the measured spectra are seen to be closed. The measured signal can be seen to show low amplitude in their spikes within the frequency band of 40–55 MHz. The reason could be from the effect of other conductors, which are not involved in the measurements. As it can be observed, the measured spectrum exhibits some bias within the frequency band of 55–100 MHz with a steep notch at 80 MHz. The reason is probably attributed to the measuring instruments as indicated earlier.

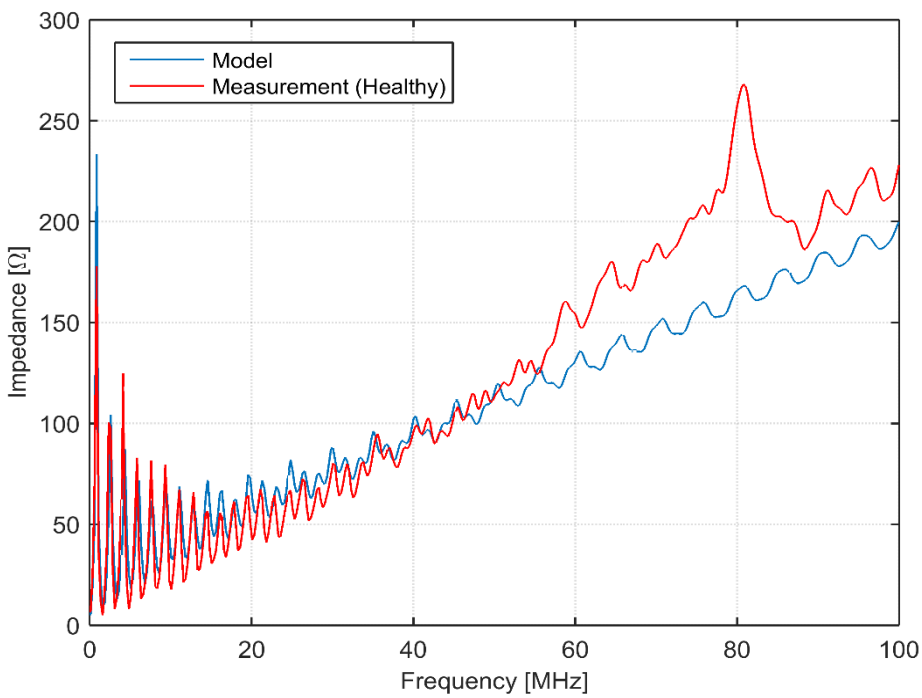

Figure 6.16. Input-impedance measurements and modelled spectra of phase-to-ground (L1, PE) coupling faulty AMCMK cable in a short-circuit situation at frequency band 100 kHz–100 MHz.

6.2 Analysis of Input Impedance Response Models

Figure 6.16 illustrates the input impedance modeled spectra of all open-circuit L1, L2 for both healthy and faulty situations. Just as it was seen in the measurements (see Figure 4.2), the modeled spectra visually shows many similarities in the frequency range of 100 kHz–30 MHz. The difference between the spectra becomes much visible after 30 MHz. Both the healthy cable and the faulty cable modeled spectra regarding measurement from P50, thus, **Case B** in Figure 4.1 exhibits low amplitude spikes compared to the others ('L1L2 faulty', 'L1L2_30_oc and L1L2_Salt_oc') as seen in Figure 6.16. While in the same frequency band of 30 –100 MHz, the modeled spectra for the 'L1L2' (faulty), 'L1L2_30_oc' and 'L1L2_Salt_oc' are similarly closed with relatively high amplitude and wider spikes. The spectrum for L1L2 (faulty) models visually shows the highest amplitude spikes followed by 'L1L2_30_oc' and 'L1L2_Salt_oc' models spectra respectively.

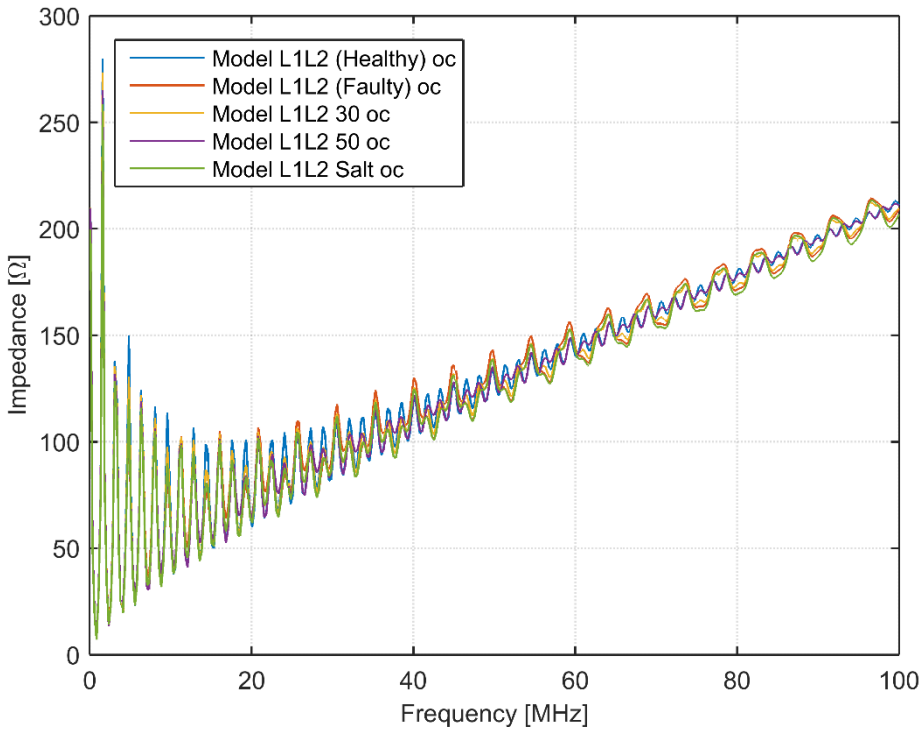

Figure 6.16. Input-impedance modelled spectra of phase-to-phase (L1, L2) coupling healthy and faulty AMCMK cable in all open-circuit situation at frequency band 100 kHz–100 MHz.

Figure 6.17 shows the input impedance of phase to phase (L1, L2) coupling spectra for both healthy and faulty short-circuit situation. The comparison of both spectra reveals many visual similarities at the frequency band of 100 kHz–18 MHz. In the frequency band of 18–100 MHz the difference between the healthy and faulty model spectra becomes visible. While the faulty model spectrum exhibits higher wider spikes, the healthy model spectrum shows rather lower and narrow spikes.

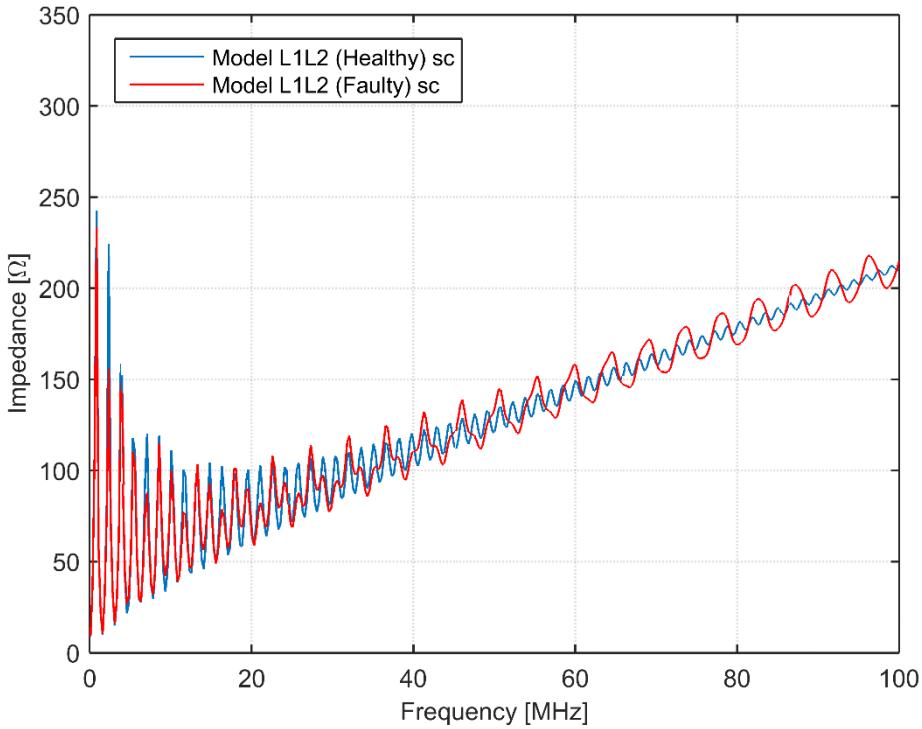

Figure 6.17. Input-impedance modelled spectra of phase-to-phase (L1, L2) Healthy and Faulty AMCMK cable in a short-circuit situation at frequency band 100 kHz–100 MHz.

Figure 6.18 illustrates input impedance spectra of phase to ground (L1, PE) coupling for both healthy and faulty models in an open-circuit situation. Comparison between both spectra shows quite similarities within the frequency band of 100 kHz–20 MHz. As the frequency increases the faulty modelled spectrum exhibits wider spikes with higher amplitude compared to the healthy model spectra. The heathy modelled spectra continue to exhibits consistent narrow spikes but lower amplitude throughout the frequency range under consideration as it attenuates

faster than the fault spectrum. Both healthy and faulty model spectra are also visually aligned within the same frequency band.

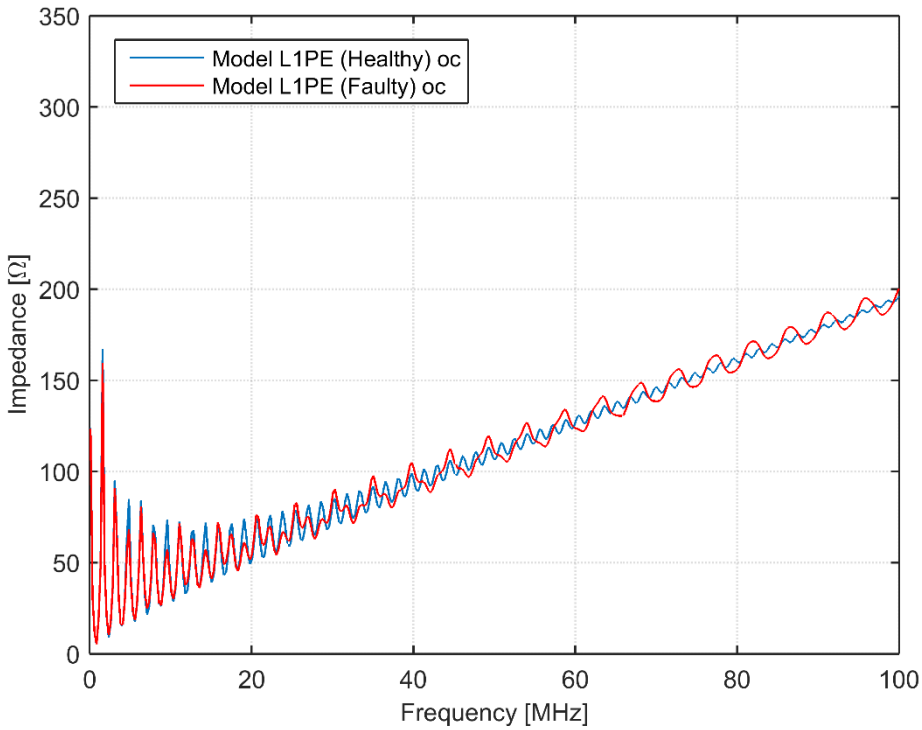

Figure 6.18. Input-impedance modelled spectra of phase-to-ground (L1, PE) coupling healthy and faulty AMCMK cable in an open-circuit situation at the frequency band of 100 kHz–100 MHz.

In Figure 6.19 the input impedance modelled spectra of phase to ground (L1, PE) coupling for both healthy and faulty models in a short-circuit situation is also illustrated. Both spectra show many visual similarities within the frequency band of 100 kHz–20 MHz with similar spikes. In the frequencies higher than 20 MHz, the faulty model spectrum begins to show wider spikes with comparatively higher amplitude than in the healthy modelled spectrum throughout the frequency range under consideration. Similar to the Figure 6.18 both the fault spectra and the healthy spectra are visually aligned.

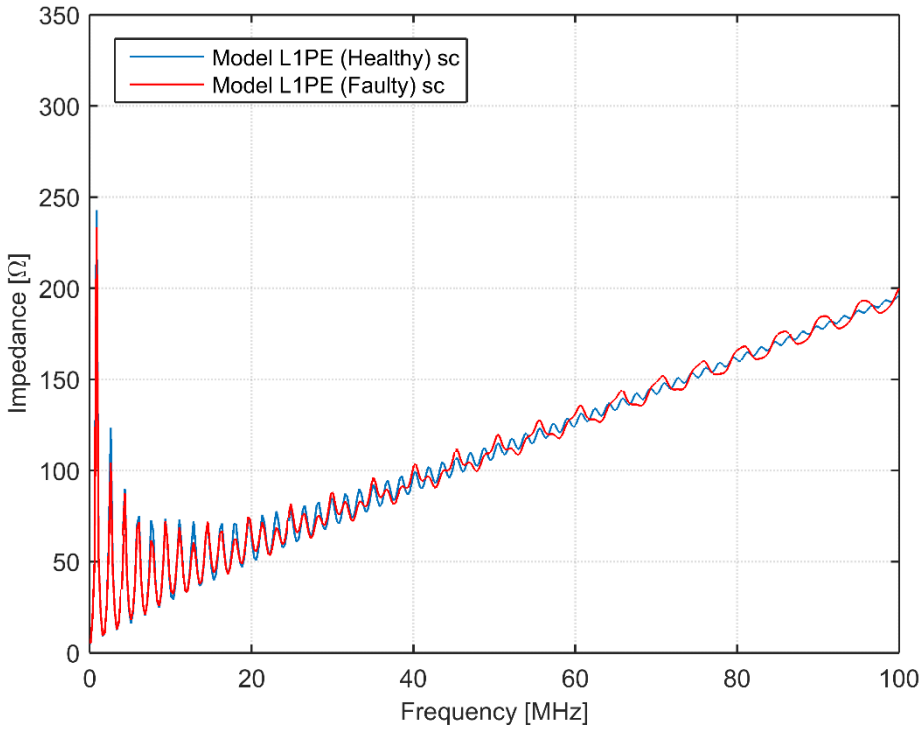

Figure 6.19. Input-impedance modelled spectra of phase-to-ground (L1, PE) coupling healthy and faulty AMCMK cable in a short-circuit situation at frequency band 100 kHz–100 MHz.

6.3 Cross Correlation Analysis

Cross correlation analysis is performed between the healthy cable measurements and their respective faulty cable modeled spectra as it can be seen from Table 6.3.The purpose of this analysis is to determine the degree of similarity between the measurements and the models. In Table 6.3, the resulting normalization values with scales option (‘1’) from the simulation are listed. According to Table 6.3, the cross correlation with the highest normalization value (‘1’) shows the most similar spectra. This can be seen in the open circuit case, where various fault modeled spectra are being compared with the same healthy measurements spectra in order to determine the degree of similarity of the models to the measurements. Since all the open circuit spectra visually look very similar, performing cross correlation between them and the healthy measurement show their degree of closeness to the measurement spectrum by their normalization values as listed in Table 6.3.

Table 6.3. Shows cross-correlation between the measurements and models spectra. This is performed to show the degree of similarity between the measurements and the modelled spectra. The cross correlation with the highest normalization value shows the most similar spectra. Ideally, the most similar spectra have normalization value of one.

Cross Correlated Spectra	**Normalization Values Between Measurements & Models Spectra**
Open-circuit (phase to phase)	
L1, L2(Healthy measurement) & L1, L2 (Healthy model)	0.9566
L1, L2(Healthy) & L1, L2 (Faulty)	0.9559
L1, L2(Healthy) & L1, L2 _30 (Faulty)	0.9566
L1, L2(Healthy) & L1, L2 _50 (Faulty)	0.9570
L1, L2(Healthy) & L1, L2 _Salt (Faulty)	0.9560
Short-circuit (phase to phase)	
L1, L2(Healthy) & L1, L2 (Healthy)	0.9907
L1, L2(Healthy) & L1, L2 (Faulty)	0.9904
Open-circuit (phase to ground)	
L1, PE(Healthy) & L1, PE(Healthy)	0.9659
L1, PE (Healthy) & L1, PE (Faulty)	0.9660
Short-circuit (phase to ground)	
L1, PE(Healthy) & L1, PE (Healthy)	0.9860
L1, PE(Healthy) & L1, PE (Faulty)	0.9861

The cross correlation between the phase to phase (L1, L2) healthy measurement and the phase to phase (L1, L2 _50) faulty model spectra in the **Case B** case, thus measurements from the cable end P50 (see Figure 4.1) shows the most similar spectra with the highest normalization value in the open circuit situation. While the cross correlation between the phase to phase (L1, L2) healthy measurement and the phase to phase (L1, L2) faulty model spectra in the **Case A** case shows the least similar spectra in the open-circuit situation. In the short circuit case, the cross correlation between L1, L2 healthy measurement and L1, L2 healthy model had the highest normalization value. In the case of phase to ground coupling, the cross correlation between the L1, PE healthy coupling, and the L1, PE faulty coupling yielded the higher normalization value in both the open-circuit and the short circuit

situations. The importance of the cross correlation is to enable accurate identification of all the faults types, especially where visual identification is no more reliable.

7 Conclusion

In this thesis, models for both healthy and faulty cables have been modeled and tuned to characterize the input impedance measurements of each open and short - circuit fault cases under consideration. The algorithm implemented in this work is based on broadband impedance spectroscopy (BIS) simulated in a Matlab environment. BIS is a novel approach for diagnosing, prognosis and estimating faults location in a cable. It is based on the measurement of broadband impedance spectrum of the power cable [12].

In all, the following models are designed. First, the model for the healthy cable in both an open-circuit and short-circuit situation during phase-to-phase (L1, l2) coupling are designed and tuned by using the cable characteristics derived from the input impedance measurements. Next, the model for the healthy cable in both an open-circuit and a short-circuit situation during phase to ground (L1, PE) coupling are also designed and tuned. The spectra for the aforementioned models and their respective measured spectra are visually similar.

In addition, the fault models for the various fault conditions are also designed. First, the open-circuit phase to phase fault in (LI, L2) coupling is designed base on input impedance measurements analysis performed in Chapter 4. The model consists of LC circuit connected in parallel to the cable. The models were in inserted in the cable models at the various fault locations. In the open-circuit situation, there are four different fault cases of L1, L2 coupling involved as presented in Table 4.2. The same model is tested on all of them but the values for the model parameters are tuned for each fault scenario. The resulted spectrum for each fault visually fits with their respective measured input impedance spectra.

In the case of the open-circuit fault regarding L1, PE coupling, an RLC circuit is designed and tested based on the same algorithm for the healthy cable. The resulting input impedance response spectra visually fit with the measured spectra except for some little distortion in the measured spectra, which is presumed to be the effect of the other two conductors not used in the input impedance measurements had on the measurements.

In the short-circuit case, the same model was designed for both phase to phase (L1, L2) coupling and phase to ground (L1, PE) coupling, consisting of RL circuits in series connection with the conductor. Their resulting modeled spectra fit with their respective input impedance measurements after each model parameters are tuned.

To determine the degree of similarity between the healthy cable measurements spectra and their respective faulty cable models spectra, a cross correlation analysis is performed and their normalization values are then calculated. The spectra with the highest normalization values are the most similar.

In this study, all the healthy and faulty cable cases are characterized and each cable and fault characteristics could be integrated as a software algorithm in a modern broadband power line communication modems, which uses orthogonal frequency-division and multiplexing (OFDM) as a channel access method. With OFDM, it possible to sweep through a wide frequency band as already used in this study. Finally, as it can be observed in all the measurements spectra discussed in Chapter 6, the behavior of the spectra above 50 MHz is unpredictable, based on that it is recommended that the future work should be limited to a frequency range up to 50 MHz.

References

[1] Philipps H., 2000 “Development of a statistical model for powerline communication channels,” in Proc. ISPLC, 2000, pp. 153–162.

[2] Prasad, T.V., Srikanth, S., Krishnan, C.N., Ramakrishna, P.V., 2006 “Wideband characterization of low voltage outdoor powerline communication channels in India,” presented at the Int. Symp. Power

[3] Järventausta, P., Verho, P., Partanen, J., Kronman, D., (2011). Finnish smart grids – A migration from version one to the next generation. In: CIRED (International Conference and Exhibition on Electricity Distribution), 21st International Conference on Electricity Distribution. Frankfurt, Germany, 6-9 June 2011.

[4] Begovic, M.M. Electrical Transmission Systems and Smart Grids: Selected Entries from the Encyclopedia of Sustainability Science and Technology. [E-book] Springer New York: New York, NY: 2013. Available through: Lappeenranta University of Technology Library website. http://ezproxy.cc.lut.fi/login?url=http://dx.doi.org/10.1007/978-1-4614-5830-2 [Accessed 12 May 2015].

[5] Renesas Electronics Corporation, 2010. Effort to Implement Smart Grids. [online] Available at: <http://www.renesas.eu/ecology/eco_society/smart_grid/> [Accessed 22 October 2015].

[6] Densley, J., "Ageing mechanisms and diagnostics for power cables - an overview," IEEE Electrical Insulation Magazine, vol. 17, no. 1, pp. 14–22, Jan/Feb 2001.

[7] Rogovin, D., Lofaro R., ‘Evaluation of the Broadband Impedance Spectroscopy Prognostics/Diagnostics Technique for Electric Cables Used in Nuclear Plants’, U.S. Nuclear Regulatory Commission Office of Nuclear Regulatory Research, Washington, June 2006, USA.

[8] Zwane, F., Afullo, T.J.O., 2014. An Alternative Approach in Power Line Communication Channel Modelling:" Progress in Electromagnetics Research C. [e-journal] 47(85–93), .Available through: Live Wire Innovation. <http://www.jpier.org/pierc/pier.php?paper=13121303> [Accessed 20th Oct, 2015]

[9] Zhu, W., Zhu, X. Lim, E., Huang, Y., 2013. State-of-art Power Line Communications Channel Modelling:" First International Conference on Information Technology and Quantitative Management. [e-journal] 17(563–570), .Available through: Science Direct.

[10] Aloha, J., 2003. Applicability of Power-Line Communications to Data Transfer of on-Line Condition Monitoring of Electrical Drives, Lappeenranta University of Technology, Lappeenranta, ISBN 951-764-783-2

[11] Kosonen, A., 2008, Power line communication in motor cables of variable-speed electric drives-analysis and implementation. Ph. D. Lappeenranta University of Technology, Lappeenranta. ISBN 978-952-214-641-0

[12]Pinomaa, A., Ahola, J., Kosonen, A., Ahonen, T., 2015. Diagnostics of low-voltage power cables by using broadband impedance spectroscopy. In: Power Electronics and Applications (EPE'15 ECCE-Europe), 2015 17th European Conference. Geneva, 8-10 Sept. 2015. Switzerland: IEEE.

[13] Dhekale P.M., Bhise S.S., Deokate N.R., 2015. Underground Cable Fault Distance Locator. [e-journal] 2(18). 1. Available through: International Journal of Innovations in Engineering Research and Technology < http://www.ijiert.org/vol_iss.php?id=7> [Accessed 7th Nov, 2015]

[14] Gajbhiye, S., Karmore, S.P., 2013. A critical comparison of reflectometry methods for location of wiring faults: Cable Fault Monitoring and Indication: A Review. [e-journal] 2(4). Available through: IJCSN International Journal of Computer Science and Network. < http://arxiv.org/ftp/arxiv/papers/1309/1309.5457.pdf> [Accessed 5th Nov, 2015]

[15] Hernández, C.P., 2012. Channel Estimation and On-Line Diagnosis of LV Distribution Cabling Available at: <uk.bl.ethos.489114> [Accessed 30.08.2015].

[16] Sidhu, T.S., Xu, Z., 2009. Detection and Classification of Incipient Faults In underground Cables in Distribution Systems. In: Electrical and Computer Engineering, 2009. CCECE '09. Canadian Conference. St. John's, NL, Canada, 3–6 May 2009. Canada: IEEE.

[17] Buchholz, V., 2004. Finding the Root Cause of Power Cable Failure. Electric Energy, [online] Available at :< http://www.electricenergyonline.com/show_article.php?article=186> [Accessed 5th Nov 2015]

[18] Geisler, H., Guinee. R. A., (2009), "A novel pseudonoise tester for transmission line fault location and identification using pseudorandom binary sequences Multicore Power Cable Troubleshooting. [Accessed 4th Nov., 2015].
[19] Neus, C., 2011, Reflectometric Analysis of Transmission Line Networks. Ph. D. Vrije Universiteit Brussel, Brussels. ISBN 978-94-9069-558-3.
[20] IEEE, 2007. Std 1234-2007 IEEE Guide for Fault-Locating Techniques on Shielded Power Cable Systems. New York: The Institute of Electrical and Electronics Engineers, Inc.
[21] Texas Instruments Incorporated, 2000. Application Bulletin: Partial Discharge Testing: What It Is and What It Means. [online] Available at :< http://www.ti.com/lit/an/sboa045/sboa045.pdf> [Accessed 5th Nov, 2015].
[22] Laughton, M.A., Warne, D. F. Electrical Engineering Reference book. [E-book] Elsevier Science: Oxford: 2003. Available through: Lappeenranta University of Technology Library website
[23] Furse, C., Chung, Y.C., Lo, C., Pendayala, P., 2006. A critical comparison of reflectometry methods for location of wiring faults: Smart Structures and Systems. [e-journal] 2(1). Available through: Live Wire Innovation. < http://cdn.livewireinnovation.com/pdf/A-Critical-Comparison.pdf> [Accessed 5th Nov, 2015]
[24] Renato Orta (2012) - Transmission Line Theory http://personal.delen.polito.it/Renato.Orta/PassOpticalComp/TransmissionLinesLecture-Notes Nov2012.pdf [Accessed 15/03/2015]
[25] Guinee, R.A. (2012), "A novel pseudonoise tester for transmission line fault location and identification using pseudorandom binary sequences, “Defect and Fault Tolerance in VLSI and Nanotechnology Systems (DFT), 2012 IEEE International Symposium on , vol., no., pp.227. [Accessed 20th Oct., 2015].
[26]Willis, H. L., Schreiber R. R., “Aging Power Delivery Infrastructures”, Second Edition Volume 35 of Power Engineering (Willis). [E-book] CRC Press, 2013: Boca Raton: 2013, pp. 384. Available through: https://books.google.fi/books?id=4WbNBQAAQBAJ&printsec=frontcover&source=gbs_ge_summary_r&cad=0#v=onepage&q&f=false [Accessed 2nd Nov. 2015]

[27] Draka NK Cables Ltd, "MCMK 4-core: 1 kV power cable with PVC insulated aluminum conductors," [Online]. Available: [Accessed 18th Oct., 2015]
[28] Draka NK Cables Ltd, "MCMK 44 ½-core: 1 kV power cable with PVC insulated aluminum conductors," [Online]. Available: http://www.draka.ee/public/product/AMCMK%204%201-2.pdf [Accessed 18th Oct., 2015]
[29] Nexans Finland, “AXMK 1 kV 4-conductor” [Online]. Available: http://www.nexans-fi.com/eservice/Finland-en/navigate_291399/AXMK_1_kV.html. [Accessed 18th Oct, 2015].
[30] Yong-Hwa Kim, "Multipath Parameter Estimation for PLC Channels Using the GEESE Algorithm," Power Delivery, IEEE Transactions on, vol. 25, pp. 2339-2345, Oct. 2010.
[31] Tlich, M., Zeddam, A., Moulin, F., and Gauthier, F., "Indoor power-line characterization up to 100 MHz – Part II: One-parameter deterministic model," IEEE Trans. on Power Delivery, 23(3), 1392–1401, Jul. 2008
[32] Laguna, G., Barron, R. Prieto, A., 2010 : ―Wavelet-based Improvement for Channel Estimation in a Power-line Communication Environment Impaired by Impulsive Noise,‖ In IEEE Electronics, Robotics and Automotive Mechanics Conference 2010, CERMA, p.p. 523–528, México, 2010.
[33] Raugi, M., Tucci, M., "Power-line communications channel estimation and tracking by a competitive neural network," Consumer Electronics, IEEE Transactions on, vol. 52, pp. 1213-1219, Nov. 2006
[34] Zimmermann M, Dostert K. A Multi-Path Signal Propagation Model for the Power Line Channel in the High Frequency Range. <http://www.sciencedirect.com/science/article/pii/S1877050913002056 > [Accessed 21th Oct, 2015], Vol. 47, Issue 11, Nov. 2009, p. 26–35.
[35] Ohki Y., Yamada T., Hirai N., ’Diagnosis of Cable Aging by Impedance Spectroscopy’, Proc. Electrical Insulation and Dielectric Phenomena (CEIDP), 16-19 Oct., Cancun, 2011, pp. 24–27.
[36] Weinstein S., ‘The History of Orthogonal Frequency-Division Multiplexing’, IEEE Communications Magazine

[37] Xiaohui Qin; Hong Shen; Qinyong Zhou; Qiang Guo; Bin Zheng; Zutao Xiang; Liangeng Ban, "Transmission-line theory based study on voltage distribution along the line and the disposition scheme of series capacitors of UHV transmission lines with series capacitors," Power System Technology (POWERCON), 2010 International Conference on , vol., no., pp.1,8, 24-28 Oct. 2010, doi: 10.1109/POWERCON.2010.5666658

Appendix I.

Figure 1(a). Algorithm for cable and fault model (Open-circuit)

```
function [Zin] = TLL(f,cable_len)% f frequency,cable length
% Cable characteristics( Distributed parameters)
l_m=249e-9;
c_m=138e-12;
r_m=1.6/10000.*sqrt(f);
g_m= 0.1.*c_m.*f;
fault_loc=17;
% velocity of propagation typical
vp=0.535.*3e8;
% Characteristic impedance vector
Z0=42;
% Attenuation coefficient vector
alfa = 0.5*1e-6.*f.^0.61;
% Propagation coefficient vector
beta = 2*pi*f./vp;
% Propagation constant
gamma =alfa + j*beta;
% Fault circuit charactristics( variable parameters)
Zc=(1/(2*pi*f.*c_m));   % Capacitive reactance
Zl=2*pi*f.*l_m;         % Inductive reactance
Zf=(Zc*1.5+Zl*0.2);     %Fault resistance(Zc+Zl*0.4);%
% The impedance of the rest of the cable at the cable fault location
Zcable = Z0.*coth(gamma.*(cable_len-fault_loc));%33
% The load impedance at the location of failure
% Zload = ( Zcable.*Zf )./(Zcable + Zf);
Zload =Zcable.*100e9;
% Matrix for the first part of the cable befor fault
TL1(1,1)=cosh(gamma.*(fault_loc));
TL1(1,2)=Z0.*sinh(gamma.*(fault_loc));
TL1(2,1)=(1/Z0).*sinh(gamma.*(fault_loc));
TL1(2,2)=TL1(1,1);
% Matrix for the second part of the cable after fault
TL2(1,1)=cosh(gamma.*(cable_len-fault_loc));
TL2(1,2)=Z0.*sinh(gamma.*(cable_len-fault_loc));
TL2(2,1)=((1/Z0).*sinh(gamma.*(cable_len-fault_loc)));
TL2(2,2)=TL2(1,1);
% Fault circuit matrix (shunt impedance at the fault location)
TL3(1,1)=1;
TL3(1,2)=0;
TL3(2,1)=(1/Zf);
TL3(2,2)=TL3(1,1);
% Cascading together various parts of the transmission line
% TL=TL1*TL2;               % For healthy cable
TL=TL1*TL3*TL2;             % For faulty cable
% Input impedance
Zin=((TL(1,1).*Zload)+(TL(1,2)))/((TL(2,1).*Zload)+(TL(2,2)));
end
```

Appendix I

Figure 1(b). Algorithm for cable and fault model (Open-circuit)

```
% Healthy cables
MCMK_healthy_L1L2_oc = load('RMAV.dat');
% Cables with 2nd degree fault and being 17 in water pool
MCMK_2dgf_17h_L1L2_oc = load('RMAV_2dgf_17h.dat');
cable_len=50;
f=100e3:100:100e6;
bias = zeros(401,1);
bias = 170/100e6.*f;
i=1;
for f=100e3:100:100e6;
    frq(i)=f;

    Zin(i)=TLL(f,cable_len);

    i=i+1;

end
figure(1)
% plot(frq,abs(Zin)+bias,MCMK_healthy_L1L2_oc(:,1),MCMK_healthy_L1L2_oc(:,2),'r');
plot(frq,abs(Zin)+bias,MCMK_2dgf_17h_L1L2_oc(:,1),MCMK_2dgf_17h_L1L2_oc(:,2),'r');
axis([0 100e6 0 350]);
% legend('Model','Measurement (Healthy)')
legend('Model','Measurement (Fault)')
xlabel('Frequency [Hz]');
ylabel('Impedance [\Omega]');
grid on
```

Appendix I

Figure 2(a). Algorithm for cable and fault model (Short-circuit)

```
function Zin = TLSC(f,cable_len)% f frequency,D cable length
l_m=249e-9;
c_m=138e-12;
r_m=(1.6)/10000.*sqrt(f);
g_m= 0.1.*c_m.*f;
fault_loc=17;
% velocity of propagation typical
vp=0.520.*3e8;
% Characteristic impedance vector
Z0=42;
% Attenuation coefficient vector
alfa = 0.5*1e-6.*f.^0.61;
% Propagation coefficient vector
beta = 2*pi*f./vp;
% Propagation constant
gamma =alfa + j*beta;
% Fault circuit charactristics( variable parameters)
Zr=r_m;                  % Resistance
Zl=2*pi*f.*l_m;          % Inductive reactance
Zf=(Zl*0.35+Zr*10);      % Fault impedance
% The impedance of the rest of the cable at the cable fault location
Zcable = Z0.*tanh(gamma.*(cable_len-fault_loc));
% The load impedance at the location of failure
% Zload =(( Zcable.*Zf)./(Zcable + Zf));
Zload =0;
% Matrix for the first part of the transmission line
TLS1(1,1)=cosh(gamma.*(fault_loc));
TLS1(1,2)=Z0.*sinh(gamma.*(fault_loc));
TLS1(2,1)=(1/Z0).*sinh(gamma.*(fault_loc));
TLS1(2,2)=TLS1(1,1);
% Matrix for the second part of the transmision line
TLS2(1,1)=cosh(gamma.*(cable_len-fault_loc));
TLS2(1,2)=Z0.*sinh(gamma.*(cable_len-fault_loc));
TLS2(2,1)=((1/Z0).*sinh(gamma.*(cable_len-fault_loc)));
TLS2(2,2)=TLS2(1,1);
% Fault circuit matrix (shunt impedance at the fault location)
TLS3(1,1)=1;
TLS3(1,2)=Zf;
TLS3(2,1)=0;
TLS3(2,2)=TLS3(1,1);
% Cascading together various parts of the transmission line
% TLS=TLS1*TLS2;
TLS=TLS1*TLS3*TLS2;
% The total system impedance
Zin=((TLS(1,1).*Zload)+(TLS(1,2)))/((TLS(2,1).*Zload)+(TLS(2,2)));

end
```

Appendix I

Figure 2(b). Algorithm for cable and fault model (Short-circuit)

```
% Healthy cables
MCMK_healthy_L1L2_ss = load('RHOS.dat');
MCMK_healthy_L1PE_ss = load('RPOS.dat');
% Cables with 2nd degree fault and being 17 in water pool
MCMK_2dgf_17h_L1L2_ss = load('RMOS_2dgf_17h.dat');
MCMK_2dgf_17h_L1PE_ss = load('RPOS_2dgf_17h.dat');

cable_len=50;
f=100e3:100:100e6;
bias = zeros(401,1);
bias = 170/100e6.*f;
i=1;
for f=100e3:100:100e6;
    frq(i)=f;
    Zin(i)= TLSC(f,cable_len);
    i=i+1;

end
figure(1)
% plot(frq,abs(Zin)+bias,MCMK_healthy_L1L2_ss(:,1),MCMK_healthy_L1L2_ss(:,2),'r');
plot(frq,abs(Zin)+bias,MCMK_2dgf_17h_L1L2_ss(:,1),MCMK_2dgf_17h_L1L2_ss (:,2),'r')
axis([0 100e6 0 350]);
legend('Model','Measurement (Fault)');
xlabel('Frequency [Hz]');
ylabel('Impedance [\Omega]');
grid on
```

Appendix I

Figure 3. Algorithm for cable and fault model (Short-circuit)

```
 clc, clear all
MCMK_healthy_L1L2_oc = load('RMAV.dat');
MCMK_healthy_L1L2_ss = load('RHOS.dat');
MCMK_healthy_L1PE_oc = load('RPAV.dat');
MCMK_healthy_L1PE_ss = load('RPOS.dat');

cable_len = 50;
freqs =(1000:100:99000000);

l_m = 249e-9;
c_m = 138e-12;
r_m = 1.6/10000.*sqrt(freqs);
g_m = 0.1.*c_m.*freqs;
vp = 0.535.*3e8;

Z0= sqrt((r_m+l_m)/(g_m+c_m))

% Attenuation coefficient vector
alfa = 0.5*1e-6.*freqs.^0.61;

% Propagation coefficient vector
beta = 2*pi*freqs./vp;

% Propagation constant
gamma = alfa + j*beta;

bias = zeros(401,1);
bias = 170/100e6.*freqs;

%for i=1:50,

    Zcable = Z0.*coth(gamma.*(cable_len));

    % The load impedance at the location of failure

    Zload =Zcable.*cable_len;

    % The total system impedance

    Zin = Z0.*(Zload+Z0.*tanh(gamma.*cable_len))./(Z0+Zload.*tanh(gamma.*cable_len));

 figure

 plot(freqs./1,abs(Zin),MCMK_healthy_L1L2_oc(:,1),MCMK_healthy_L1L2_oc(:,2));
 axis([0 30e6 0 400])
 legend('Model','Healthy L1L2oc')
 xlabel('Frequency (MHz)');
 ylabel('Impedance (ohm)')
 grid;
```

Appendix II.

Table 1. Cable faults diagnosed from series resistance (continuity) and shunt resistance measurement

Fault diagnosis from series resistance (continuity) measurements

R	Problem	Solution
$R < 5\ \Omega$	High-resistance shunt fault.	Measure fault shunt resistance.
$5\ \Omega < R < 1\ M\Omega$	High-resistance shunt fault. Concentric neutral corrosion. Corroded termination or splice. Corroded or burnt conductor. Water soaked, burnt cable section.	Measure fault shunt resistance. A HV fault-locating technique or a bridge technique for three conductor cables must be used. With a TDR, the exact problem shall be determined and the appropriate fault-locating procedure and technique selected.
$R > 1\ M\Omega$	Sealed off conductor. Separated splice or termination. Missing concentric or sheath.	With a TDR, the exact problem shall be determined and the appropriate fault-locating procedure and technique selected.

Fault diagnosis from shunt resistance measurements

R	Problem	Solution
$R > 1\ M\Omega$	High-resistance shunt fault. Disintegrated concentric. Separated splice. Open conductor.	A HV fault-locating technique such as arc reflection, surge pulse, or voltage decay must be used. With a TDR, the exact problem shall be determined and the appropriate fault-locating procedure and technique selected.
$R < 1\ M\Omega$	With an ohmmeter the fault resistance, *R*, shall be measured.	
$R > 500\ \Omega$	Solid shunt fault.	A HV fault-locating technique or a bridge technique for three conductor cables shall be used.
$5\ \Omega < R < 500\ \Omega$	Destroyed and burnt cable section. Conductive path between conductors. Water soaked fault.	With a TDR, the exact problem shall be determined and the appropriate fault-locating procedure and technique selected.
$R < 5\ \Omega$	Bolted fault. Grounds connected. Transformer connected.	With a TDR, the exact problem shall be determined and the appropriate fault-locating procedure and technique selected.

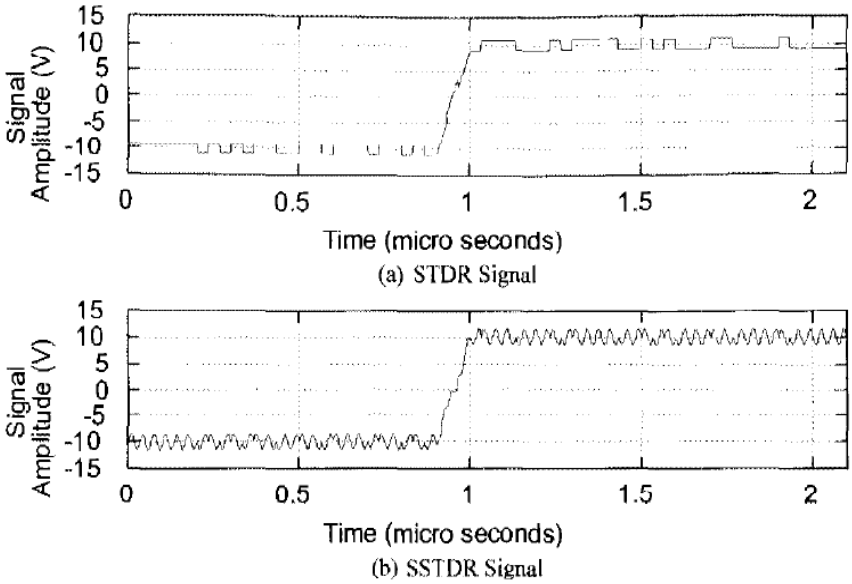

Figure 1 Spectra (a) and (b) illustrate incident signals of STDR and SSTDR [7]

Appendix II

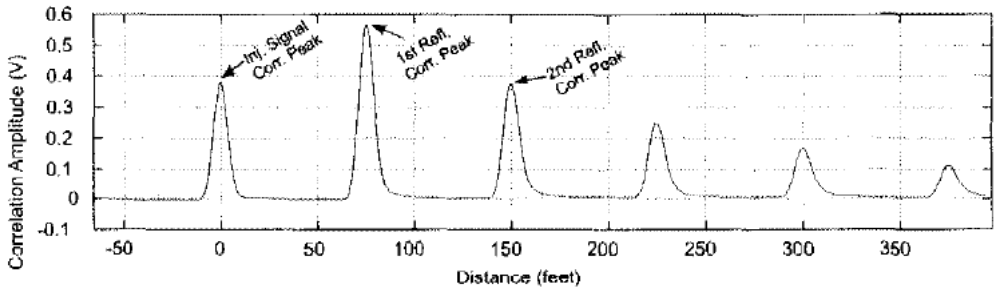

(c) Correlation response of STDR signal

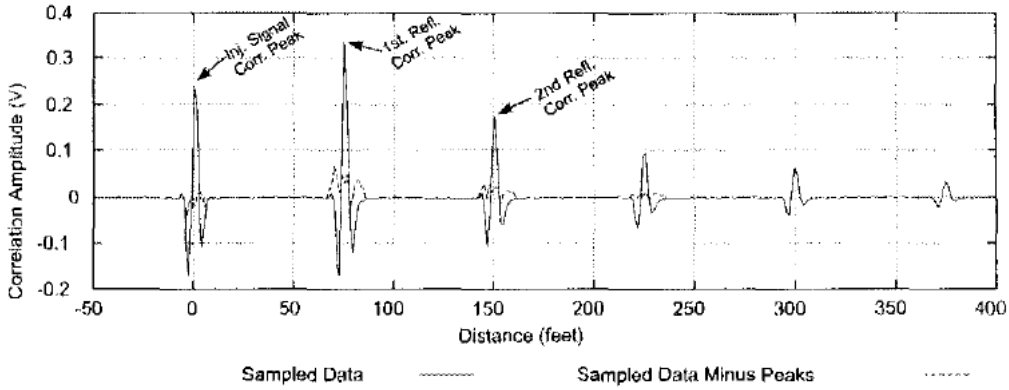

(d) Correlation response of SSTDR signal

Figure 2 (a) and (b) shows a correlated signals of STDR and SSTDR [7]

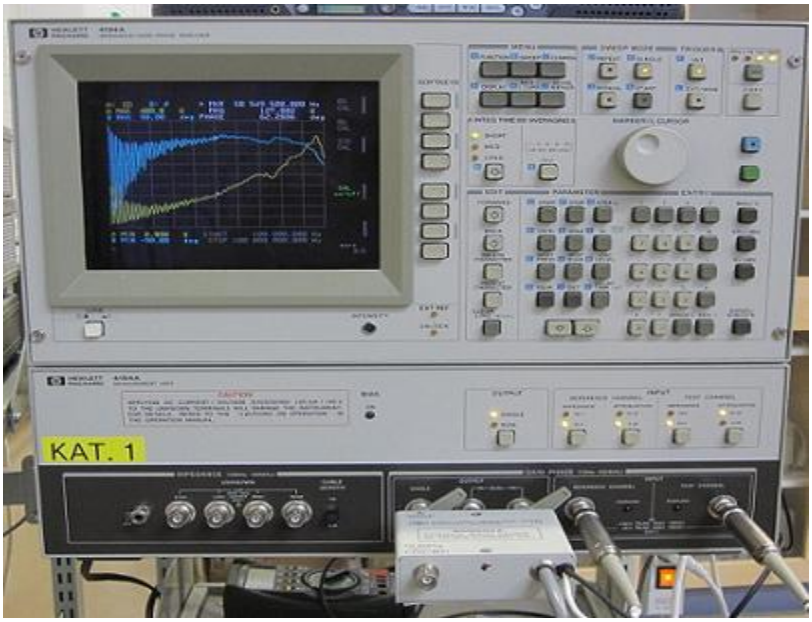

Figure 3 Impedance Analyser HP4194A used in the phase impedance measurements